

From the Institute of Anatomy and Cell Biology, Department of Neuroanatomy

Faculty of Medicine, University of Saarland,

Homburg/Saar

Characterization of exocrine secretory glands in the digestive tract of CSP α knockout mice

Inaugural Dissertation presented to the Faculty of Medicine, University of Saarland, Homburg, Germany, in order to obtain the degree of Dr. med.

By: Josif Mirceski

Born on 16.10.1979, in Prilep, Republic of Macedonia

Homburg

2008

Date of promotion:

Dean:

Correspondent:

Table of Contents

1. Summary	12
2. Introduction.....	14
2.1. Molecular anatomy of CSP proteins.....	14
2.1.1. J-domain	15
2.1.2. Linker domain.....	15
2.1.3. The cysteine string	16
2.1.4. The variable C-terminus.....	16
2.1.5. The N- terminus	17
2.2. Hypothesis on CSP function.....	17
2.2.1. Involvement in Ca ²⁺ channel function.....	17
2.2.2. Regulation of exocytosis	18
2.2.3. Chaperone function.....	20
2.3. Analysis of CSP function in CSP deficient flies	21
2.4. Analysis of CSP α function in CSP α KO mice.....	21
2.5. Exocrine secretory glands in the gastrointestinal tract	25
2.5.1. General aspects of food digestion.....	25
2.5.2. Histology and physiology of major exocrine glands in the digestive tract.....	26
2.6. Mast cells.....	28
2.7. Aim of the present study: CSP protein and the pancreas	28
3. Materials and Methods	30
3.1. Chemicals and materials	30
3.2. Experimental animals	33
3.3. Electron microscopy	34

3.3.1.	Preparation of the solutions and buffers used for washing, fixing and embedding the tissues.....	34
3.3.2.	Preparation of Richardson Blue stain.....	36
3.3.3.	Organs harvesting, fixing and embedding for electron microscopy	36
3.3.4.	Trimming and cutting.....	39
3.3.5.	Section-contrasting	39
3.3.6.	Analysis by transmission electron microscopy	40
3.3.7.	Morphometric and statistical analysis of data.....	40
3.4.	RNA extraction and purification.....	40
3.4.1.	Parotid gland.....	40
3.4.2.	Mast cells	41
3.4.3.	Pancreas.....	41
3.4.4.	Testis	42
3.5.	Reverse transcriptase polymerase chain reaction (RT-PCR).....	42
3.5.1.	Reverse transcription	42
3.5.2.	PCR	43
3.6.	DNA extraction and purification for CSP genotyping.....	44
3.6.1.	Phenol-chloroform extraction method	45
3.6.2.	Two-step method for DNA extraction	45
3.7.	Genotyping for the wild type (WT) and knockout (KO) CSP allele	46
3.8.	Agarose gel electrophoresis.....	47
4.	Results	48
4.1.	General remarks on EM quantifications.....	48
4.2.	Qualitative and quantitative transmission electron microscopy of exocrine pancreatic acinar cells in CSP α KO and WT control animals.....	51
4.2.1.	Number of zymogen granules per acinar cell.....	53

4.2.2.	Zymogen granules diameter.....	53
4.2.3.	Serial sections, average maximum diameter and average volume of the zymogen granules	55
4.2.4.	Distribution of zymogen granules in exocrine pancreatic acinar cells .	56
4.3.	Quantitative transmission electron microscopy of parotid acinar cells in CSP α KO and WT control animals.....	58
4.3.1.	Zymogen granule diameter	60
4.3.2.	Average granule number per acinar cell	61
4.3.3.	Distribution of zymogen granules in parotid acinar cells	62
4.4.	Quantitative transmission electron microscopy of submandibular serous acinar cells in CSP α KO and WT control animals	64
4.4.1.	Zymogen granule diameter	66
4.4.2.	Average granule number per acinar cell	67
4.4.3.	Distribution of zymogen granules in submandibular serous cells	68
4.5.	Mast cells	70
4.6.	CSP isoforms genotyping.....	72
5.	Discussion	74
6.	Conclusion.....	79
7.	References	80
8.	Acknowledgements	88
9.	Curriculum Vitae.....	89

Table of figures

Figure 1: Scheme of the CSP domain structure	15
Figure 2: Schematic representation of pancreatic exocrine acinus (applicable also for parotid and submandibular glands)	26
Figure 3: Schematic representation of an acinar cell and measuring the distribution of the granules in the cell.....	49
Figure 4: Scheme of single (left) and serial sectioning (right) of the zymogen granules	50
Figure 5: The phenotype of the exocrine pancreatic acinar cells in CSP wild-type and CSP knockout animals.	52
Figure 6: Granules number in pancreatic acinar cell	53
Figure 7: Zymogen granule diameter in pancreatic acinar cells.....	54
Figure 8: Diameter and volume of zymogen granules from serial sectioning.....	56
Figure 9: Distribution of the granules in the pancreatic acinar cells.....	57
Figure 10: The morphology in the acinar cells of the parotid gland in CSP α KO and WT animals.....	59
Figure 11: Zymogen granule diameter in the parotid acinar cells	60
Figure 12: Granule number in the parotid acinar cells	61
Figure 13: Quantification of distribution of zymogen granules in parotid acinar cells	62
Figure 14: Morphology of the acinar cell from the submandibular gland of CSP wild-type and CSP knockout mice.....	65
Figure 15: Some of the heteromorphous granules in the submandibular gland of CSP knockout animals at higher magnification	66
Figure 16: Zymogen granule diameter in the submandibular acinar cells.....	67
Figure 17: Zymogen granule number per acinar cell	68

Figure 18: Distribution of the zymogen granules in the serous acinar cells of the submandibular gland	69
Figure 19: Peritoneal mast cells	70
Figure 20: Mast cells parameters quantification results	71
Figure 21: CSP Isotyping in the bone marrow mast cells	72
Figure 22: CSP Isotyping in the exocrine pancreas and the parotid gland	73

List of tables

Table 1: Chemicals and reagents used in the experimental procedures	31
Table 2: Laboratory hardware equipment.....	33
Table 3: Software packages used in the processing of the digital data	33
Table 4: Solutions and buffers (and their composition) used for washing, fixing and embedding the tissues.....	35
Table 5: Composition of the PCR mixture used for reverse transcription	42
Table 6: Composition of the PCR mixture added at step 2 of the reverse transcription	43
Table 7: Composition of the PCR mixture used for generating the second strand of the DNA	43
Table 8: Primers and their sequences used for CSP RT-PCR	44
Table 9: Thermal cycler PCR conditions used in the CSP isotyping.....	44
Table 10: Master Mix of reagents used for the WT PCR reaction.....	46
Table 11: Master Mix of reagents used for the KO PCR reaction	46
Table 12: Thermal cycler conditions used for the CSP genotyping	47

Abbreviations

α GDI	α GDP dissociation inhibitor
ATP	Adenosine triphosphate
BMMC	Bone marrow mast cells
bp	Base pairs
CSP	Cysteine string protein
CSP α,β,γ	Cysteine string protein, isoform α , β or γ
DDSA	Dodecanyl succinic anhydride
DEPC	Diethyl pyrocarbonate
DMP30	2,4-tri(dimethylaminoethyl)phenol
DNA	Deoxyribonucleic acid
dNTP	Deoxy nucleotide tri-phosphate
DTT	Dithiothreitol
EDTA	Ethylenediamine tetraacetic acid
ERG	Electroretinogram
EM	Electron Microscope, electron microscopy
EPON	Epoxy resin
GABA	γ -aminobutyric acid
GABA _B	γ -aminobutyric acid receptor type B
GAD	Glutamate decarboxylase
GDP	Guanosine diphosphate

GTP	Guanosine triphosphate
Hsc70	Heat-shock cognate of 70kDa
Hsp40	Heat-shock protein of 40kDa
Hsp70	Heat-shock protein of 70kDa
kDa	Kilodaltons
KO	Knockout
L	Lumen
LDCV	Large dense-core vesicles
N	Nucleus
NMA	Nadic methyl anhydride
NMJ	Neuro-muscular junction
OD	Optical density
PBS	Phosphate-buffered saline
PCR	Polymerase chain reaction
PFA	Paraformaldehyde
Px	Postnatal day X
r	Radius
RNA	Ribonucleic acid
rpm	Rounds per minute
RT	Room temperature
RT-PCR	Reverse transcriptase polymerase chain reaction
SGT	Small glutamine-rich TRP protein

SNARE	Soluble N-ethylmaleimide-sensitive factor attachment protein receptor
SV	Synaptic vesicle
TAE	Tris-acetate buffer with EDTA
TRP	Tetratricopeptide repeat
UA	Uranyl acetate
UV	Ultraviolet
V	Volume
VAMP	Vesicle-associated membrane protein
vGAT	Vesicular GABA transporter
WT	Wild-type

1. Summary

CSPs (cysteine string proteins) are relatively small proteins originally discovered in brain homogenates of *Drosophila melanogaster*. They are associated with the membrane of the synaptic vesicles, as well as with secretory vesicles of other, non-neuronal cell types. Since their discovery, there have been several hypothesis of their function: namely, that they are involved in regulation of voltage-dependent Ca^{2+} channels, that they regulate exocytosis and acting as a part of an Hsp70 chaperone complex.

To further study and characterize the functions of CSP, $\text{CSP}\alpha$ knockout (KO) mice were generated (Fernandez-Chacon et al. 2004). The $\text{CSP}\alpha$ KO mice are viable at birth and develop normally in the beginning, but after about two weeks of age, they stop gaining weight, suffer from vision impairments and develop fatal sensorimotor disorder. The mutant mice lacking the $\text{CSP}\alpha$ gene die at the age of ~2 months (Fernandez-Chacon et al. 2004). This late onset of the symptoms combined with the neuro-muscular junction (NMJ) and Calyx synapses' degeneration only after certain period (~2-3 weeks of age), strongly favors a chaperone function of CSP. Particularly, proteins involved in the exocytosis undergo constant cycles of assembly and disassembly. After extended usage, these proteins age and in the animals that lack the chaperone machinery, they cannot be repaired and recycled. These effects lead to the degeneration of the synapses.

CSP is found also on the secretory vesicles (zymogen granules) of the pancreatic acinar cells (Brown et al. 1998). The $\text{CSP}\alpha$ KO mice exhibit disturbances in the weight gain. These changes could be contributed to alterations in the exocrine pancreas. This study aims to look for possible alterations in the pancreatic exocrine

cells that could lead to defects of secretion of digestive enzymes and therefore disturbances in weight gain. In addition, other exocrine glands in the digestive system (parotid and the submandibular) were examined. This study shows that all of the secretory glands have structural alterations. Particularly, the exocrine zymogen granules of the mutant animals showed altered characteristics: they were bigger in diameter (pancreas, parotid and submandibular), more in number (pancreas and submandibular, but not parotid gland) and had an altered intracellular distribution (regarding the polarity of the cell) in every organ observed. Not all of the cells in the mutant animals were affected. No changes were observed in mast cells.

Mechanistically, the overall changes observed in the glands could be attributed to the inability of the cellular machinery to recycle important proteins (SNAREs, Rabs). It has been suggested that Rab3D (which interacts with a complex that contains CSP) is responsible for maintaining normal size of the granules. In addition, the inability to efficiently form SNARE complexes, therefore inability to perform exocytosis, could lead to accumulation of granules in the cell. These results favour the theory that CSP α acts primarily as a chaperone, recycling important cellular components. How exactly these changes occur at a molecular level needs to be addressed by future investigations.

2. Introduction

Cysteine-string proteins (CSP) are relatively small proteins, originally discovered in *Drosophila melanogaster* using a monoclonal antibody raised against a crude brain homogenate (Zinsmaier et al. 1990). CSPs are associated with the cytosolic face of the membranes of synaptic vesicles. They have also been localized on the membranes of secretory vesicles of chromaffin cells (chromaffin granules; Chamberlain and Burgoyne 1998), exocrine pancreatic cells (zymogen granules; Braun and Scheller 1995), insulin-containing large dense-core secretory granules of neuroendocrine β -cells (Zhang et al. 1998), and secretory granules of the rat neurohypophysis (Jacobsson and Meister 1996).

CSP proteins are ubiquitously found in the animal world. They are expressed in invertebrates as well as in vertebrates. In invertebrates, like *Drosophila*, there is one gene that codes for CSP1, as well as its C-terminal splice isoform CSP2. In mammals, there are three genes that code the three isoforms so far known- CSP α , β and γ . CSP α is ubiquitously expressed in various tissues, but highly enriched in brain. The other two isoforms, CSP β and γ are testis specific (Fernandez-Chacon et al. 2004).

2.1. Molecular anatomy of CSP proteins

CSPs are characterized by typical domain structure: they contain a J-domain at the N-terminus of the protein, a cysteine-rich string towards the C-terminus of the protein, a linker region connecting them, and the highly conserved C-terminus (Mastrogiamo and Gundersen 1995) (Figure 1).

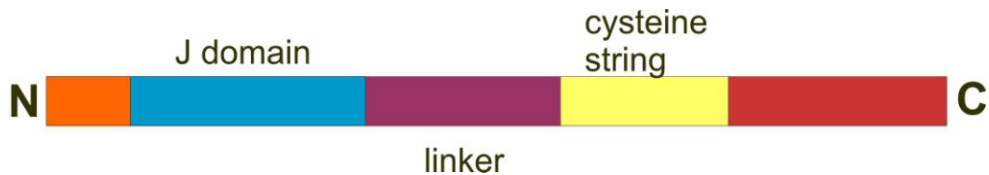


Figure 1: Scheme of the CSP domain structure

N: N-terminus, C: C-terminus

2.1.1. *J-domain*

The J-domain was initially described in bacteria (bacterial DnaJ protein) and it is the signature domain of Hsp40-type co-chaperones. It comprises a stretch of 70 amino-acids evolutionary conserved from *E. coli* to man. It is well established that the J-domain mediates binding of the Hsp40 co-chaperones to Hsp70 chaperone proteins (Caplan et al. 1993; Silver and Way 1993). So far, a considerable number of eukaryotic proteins have been found that contain a “J” domain. For most of them it has been shown that they interact with and regulate the functions of members of the Hsp70 chaperone group (Cheetham and Caplan 1998; for review, see Chamberlain and Burgoyne 2000). Several studies demonstrated that CSP interacts with Hsc70 in an ATP-dependent manner (Braun et al. 1996). This interaction that stimulates the ATP-ase activity of both Hsc/Hsp70 several fold (Chamberlain and Burgoyne 1997) is mediated by the DnaJ domain of the CSP (Braun et al. 1996; Stahl et al. 1999).

2.1.2. *Linker domain*

The linker domain (~20 amino acids) is highly conserved region, and is found between the J-domain and the cysteine string. Its function is still unknown, though it has been suggested to be important for the effects of CSP on secretion (Zhang et al. 1999).

2.1.3. *The cysteine string*

The cysteine string, after which the protein is named, contains a high number of cysteine residues (14) in a 24 amino acid span (for *Torpedo* and mammalian CSPs), which are heavily palmitoylated. This string is responsible for the localization of the CSP to the membranes of the secretory vesicles (Gundersen et al. 1994; Mastrogiacomo et al. 1994; Mastrogiacomo and Gundersen 1995; Chamberlain and Burgoyne 1998). The palmitoylation of these cysteine residues gives the protein an amphipathic structure, which could mediate the correct membrane association of the CSP (Gundersen et al. 1994). Complete depalmitoylation, however, does not displace the CSP from the membranes, indicating that palmitoylation is required for initial membrane targeting, but not stable membrane association (van de Goor and Kelly 1996; Chamberlain and Burgoyne 1998). In a recent study (Ohyama et al. 2007) it is suggested that, in *Drosophila*, the Huntingtin-interacting protein 14 (hip14) which acts as a palmitoyl transferase, is responsible for the palmitoylation of CSP. hip14 mutants show exocytic defects or nearly complete loss of synaptic transmission, and also severe mislocalization of CSP in the synapses.

2.1.4. *The variable C-terminus*

This part of the CSP is the most variable domain and strongly varies between the different CSP isoforms as well as among different species. In *Drosophila*, deletion in the C- terminus does not affect membrane targeting of the CSP (Arnold et al. 2004). Also, it has been found that the C- terminus mediates the homodimerization of CSP and its Ca²⁺-dependent interactions with the SNARE protein VAMP2, but not with its isoform VAMP3 (Boal et al. 2004).

2.1.5. *The N- terminus*

The N- terminus of the CSP is another part of the protein which is variable. Its importance is largely unknown. It has been shown that it is not required for targeting of CSP to the membranes of the vesicles (Boal et al. 2004).

2.2. *Hypothesis on CSP function*

2.2.1. *Involvement in Ca²⁺ channel function*

The first hypothesis for CSP function suggested an involvement of CSP in the regulation of Ca²⁺ channel function. Based on overexpression studies, it has been observed that CSP antisense RNA inhibits expression of the N-type Ca²⁺ channels when coinjected with *Torpedo* electric lobe mRNA into *Xenopus* oocytes (Gundersen and Umbach 1992). Furthermore, it was found that voltage-gated Ca²⁺ influx was impaired in CSP mutant *Drosophila* synapses and that neurotransmitter release could be rescued in these flies by application a Ca²⁺ ionophore (Ranjan et al. 1998). Introduction of recombinant CSP into chick nerve terminals increased Ca²⁺ channel activity (Chen et al. 2002) and CSP α may bind to vertebrate Ca²⁺ channel proteins (Leveque et al. 1998) or to G protein subunits regulating Ca²⁺ channels (Magga et al. 2000). The idea that CSP mediates the assembly or regulation of Ca²⁺ channels at the active zone is attractive in view of the localization of CSP on synaptic vesicles. This hypothesis of CSP regulating Ca²⁺-channels was tested by fluorometric Ca²⁺ measurements that demonstrated that nerve terminals from *Drosophila* CSP mutants display an increase, and not a decrease, in Ca²⁺ influx (Dawson-Scully et al. 2000) and by measurements of Ca²⁺ currents in peptidergic terminals from CSP mutant flies (Morales et al. 1999). In addition, this hypothesis was also tested in the Calyx of Held

synapse of the CSP α KO mutant mice. When investigating the presynaptic Ca²⁺ channel function in the mutant mice, no significant changes were observed (Fernandez-Chacon et al. 2004). What was observed was close similarity in the activation time course and voltage dependence of the Ca²⁺ currents.

The proposition that CSP α regulates G protein modulation of the Ca²⁺ channels was also tested in these synapses. As these synapses express presynaptic GABA_B receptors, which, when activated cause a characteristic slowing of Ca²⁺ channel opening, a selective GABA_B receptor agonist (50 μ m Baclofen) was applied. Once more, no differences between the CSP α KO mutants and the wild-type controls were observed (Fernandez-Chacon et al. 2004), implying that CSP α is not directly involved in Ca²⁺ channel function and thus not important for Ca²⁺-channel regulation.

2.2.2. Regulation of exocytosis

Based on overexpression studies, it has been suggested that CSP functions in regulating exocytosis. It has been found that CSP interacts with syntaxin and synaptotagmin in pulldown experiments (Nie et al. 1999; Evans and Morgan 2002; but see Leveque et al. 1998; Matos et al. 2000 for alternative results). Moreover, transmitter release is depressed in *Drosophila* CSP mutants despite higher than normal Ca²⁺ levels indicating a role for CSP in determining the Ca²⁺ sensitivity of secretory apparatus (Dawson-Scully et al. 2000). Furthermore, overexpression of CSP in neuroendocrine cells altered exocytosis but had no effect on Ca²⁺ channel activity (Brown et al. 1998; Chamberlain and Burgoyne 1998; Zhang et al. 1998; Graham and Burgoyne 2000).

Fernandez-Chacon et al. 2004 tested this hypothesis on Calyx of Held synapses from the CSP α KO mice, examining the initial synaptic responses, finding no significant

differences between the mutant and the wild-type mice. In addition, no significant differences were found for the synaptic responses during stimulus trains, and for the quantal properties of transmitter release, implying that CSP is not directly involved in the regulation of exocytosis. On the other hand, it has been shown that CSP α plays important role in the assembly of the SNARE complex, as the formation of this complex is impaired in the CSP α KO mice (Chandra et al. 2005).

CSP has been shown that regulates the uptake of γ -aminobutyric acid (GABA) into the synaptic vesicles (Hsu et al. 2000). CSP associates with the enzyme that synthesizes the GABA- glutamate decarboxylase (GAD) - and the vesicular GABA transporter (vGAT), indirectly through its interactions with the Hsp70 (Hsu et al. 2000, for review, see Evans et al. 2003). In these studies, it is suggested that CSP acts in the tethering of GAD to the membrane of the synaptic vesicle (SV) by its interaction with Hsc70, since Hsc70 directly binds GAD and the three are found in complex on SV membranes. Together with other proteins that bind directly to vGAT, they could form a large complex responsible for GABA filling of SV (Evans et al. 2003).

CSP has also been identified as a component of a chaperone complex containing α GDI, Hsp90 and Hsc70 (Sakisaka et al. 2002; reviewed in Evans et al. 2003). α GDI (α -GDP dissociation inhibitor) is a specific effector of the vesicle cycling of the Rab3A proteins. Rabs are a family of proteins involved in targeting and docking of vesicle fusion in all membrane trafficking events in the cell (Zerial and McBride 2001). Rab3A is a key member of this family, involved in the targeting of the SV to the presynaptic terminal plasma membrane. When the vesicle is formed, Rab3A-GTP binds to the SV membrane, and later, when the SV is fused to the plasma membrane, Rab3A hydrolyzes the GTP to GDP, thus enabling the α GDI to remove the Rab3A-GDP from the membrane (Luan et al. 1999). After that, Rab3A undergoes new cycle of GDP-

GTP exchange and is recruited to a new vesicle. On the other hand, in another study (Riedel et al. 2002) it is suggested that Rab3D is not responsible for vesicle docking, but for maintenance of normally sized granules. Rab3D KO mice exhibited increase of the zymogen granules' size in the parotid and pancreatic acinar cells, but this deletion did not show effects on the exocytosis (Riedel et al. 2002).

Being part of such a complex gives an important role to CSP in the membrane fusion events, involving it in the association and dissociation of the Rabs to and from the SV membrane.

2.2.3. Chaperone function

Based on the observation that CSP contains a DnaJ domain, another hypothesis emerges. Namely, DnaJ domains are characteristic of co-chaperones of the Hsp40 family, and they functionally collaborate with the DnaK domains of Hsc70 proteins (reviewed in Kelley 1998; Hartl and Hayer-Hartl 2002). In another study, it was shown that CSP activates the ATPase activity of Hsc70 (Braun et al. 1996; Chamberlain and Burgoyne 1997) and forms a trimeric complex with Hsc70 and a tetratricopeptide repeat protein called small glutamine-rich tetratricopeptide repeat protein (SGT, Tobaben et al. 2001). In this study, it was shown that this new member, discovered in a yeast-two hybrid screening, could bind both the CSP and the Hsc70 and simultaneously activate the ATPase activity of the Hsc70. So far, the complex CSP-Hsc70-SGT is known to catalyze the ATP-dependent refolding of denatured luciferase *in vitro* (Tobaben et al. 2001), which suggests that this could be another chaperone- co-chaperone complex. Human SGT has been shown to take important part in the cell division (Winnefeld et al. 2004), but whether this is achieved through its interactions with Hsc70 and CSP is still unknown.

This role for CSP as a compensatory chaperone to renature nerve terminal proteins that misfold during the continuous operation of the synaptic vesicle cycle is very attractive one.

2.3. Analysis of CSP function in CSP deficient flies

To analyse the functions of CSP *in-situ*, many studies were done on *Drosophila* mutants that lack CSP. In *Drosophila*, CSP is important for evoked neurotransmitter release. Most flies that lack CSP die during development, but there is still a small percentage that survives into adulthood. These survivors are characterized with a temperature-sensitive paralytic phenotype (Umbach et al. 1994; Zinsmaier et al. 1994). Studies of the neuromuscular junction of larvae from surviving mutant flies revealed that deletion of CSP severely depressed evoked neurotransmitter release at the permissive temperature and nearly abolished release at the non-permissive temperature (Umbach et al. 1994; Zinsmaier et al. 1994). These temperature-dependant effects on evoked synaptic transmission support the chaperone hypothesis of CSP function.

2.4. Analysis of CSP α function in CSP α KO mice

Recently, mice with genomic deletion of CSP α were generated (Fernandez-Chacon et al. 2004), enabling *in vivo* characterization the roles of the CSP α . These mice are viable at birth, but show progressive and rapid neurodegeneration and die at relatively young age. In the first two postnatal weeks, survival and body weight of the KO mice are not different from the WT or heterozygous littermate controls. But at two to three weeks of age the mutants show signs of progressive weakness. They stop

gaining weight at the age of P15 and later enter into lethargic state and start to die in the third postnatal week, with most of them dying in the second postnatal month. None of the KO mice survived more than 3 months. These mice are also characterized by progressive sensorimotor impairment, expressed in their muscle weakness (Fernandez-Chacon et al. 2004), and their progressive blindness (Schmitz et al. 2006).

As the CSP α KO mice are characterized by progressive neuromuscular dysfunction, they have been subject to different neurological examinations. What was obvious from these examinations is that the CSP α KO mice exhibit impaired sensorimotor performance and neuromuscular function. Namely, already at P15, they showed loss of spontaneous activity; muscle weakness manifested by lack of gripping strength; typical posture with the position of the legs like “inverted champagne bottles”; inability to stay on a turning rode; difficulties in getting up when placed on side (Fernandez-Chacon et al. 2004). All of these data suggest that the NMJ might be dysfunctional. When examining the function of the NMJ by electromyographic responses, it has been found that in the CSP α KO mice, stimulus trains elicit enhanced synaptic depression, observed already at P15, which becomes more severe at P23 and 47. The mean amplitude of the compound muscle action potentials at P15 showed no difference in the mutant mice compared to their littermate controls, but at P43 deteriorated. All of these data give strong suggestion that the CSP α KO mice have impaired function of the NMJ that becomes more severe with progressing age, and raise the question about the morphological changes in the NMJ. And, in deed, the NMJ showed changes in the morphology which become more apparent with the age. Namely, as observed with fluorescence and electron microscopy, the pre- and postsynaptic terminal of the NMJ developed normally initially, but with progressive

age and increasing demands on the synapse, the presynaptic terminal degenerated. The signs of degeneration (vacuoles, multilamellar bodies and Schwann cell protrusions) were evident at all ages examined, but occurring much more often at later stages than in young mice (at P7). It is worth noting that not all of the NMJs in the CSP α KO mice were affected by the degeneration.

In another study involving these mice, (Schmitz et al. 2006) have found similar type of age-dependent degeneration in the photoreceptors of the retina. In the initial 2 weeks of postnatal life, the retina of the CSP α KO mice shows no or little differences compared to the wild-type controls, as monitored by electroretinography, electron and fluorescence microscopy. Differences start to occur immediately after eye opening (after P14) and tend to become sharper with age. At P14, ERG responses show some differences in the mutant mice as compared to their wild-type controls, and these differences become more apparent at later stages of development, with complete abolishment of vision after 4 weeks of age.

In addition, immediately after eye opening, at P15, no dramatic changes have been observed concerning the distribution of synaptic proteins and the ultrastructural morphology of the ribbon synapses. These changes became obvious only in later stages of the development, namely at P28 and later, consisting of mislocalization of some synaptic proteins (ribeye, synaptophysin, synaptotagmin) and reduced abundance of these. The strong changes were also visible at the ultrastructural level, showing signs of severe degeneration (Schmitz et al. 2006).

It is worth noting that no changes were observed in the inner hair cells, which is due to the expression of another CSP isoform, CSP β , in these cells. This isoform on the other hand is not expressed in the retina, and in the inner hair cells is compensating the effects of the CSP α deletion (Schmitz et al. 2006).

In another study involving the CSP α KO mice (Chandra et al. 2005), it has been suggested that CSP is important for the assembly of the SNARE complexes. There it has been shown that CSP α KO mice have decreased ability for assembly of SNARE complexes.

All of these data, namely, the progressive sensorimotor impairment as obtained from the neurological examinations, the enhanced depression of stimulus response at the NMJ and its progressive morphological degeneration (Fernandez-Chacon et al. 2004), the progressive loss of vision and blindness (Schmitz et al. 2006), decreased formation of SNARE complexes (Chandra et al. 2005), combined with the previous studies (Braun et al. 1996 ; Chamberlain and Burgoyne 1997; Tobaben et al. 2001), strongly support the idea that CSP α acts as a compensatory chaperone in the presynaptic terminal at the synapse.

The Hsp70/CSP complex binds to short stretches of exposed, hydrophobic amino-acid residues, which are exposed on partially or completely unfolded proteins and/or protein intermediates. With this, they ensure the proper folding of newly synthesized proteins, as well as the refolding of denatured or partially denatured ones. This function of the Hsp70 chaperones makes them very important part of the cellular rescue machinery.

Chaperone activity is very important at the presynaptic terminal in particular, where a continuous process of exo- and endocytosis takes place. Depending on the location of the terminal in the nervous system, tens to hundreds synaptic vesicles are being exocytosed at regular or irregular intervals, utilising many different proteins responsible for the transport, priming, docking and other processes involved in the exocytosis. This regulated secretion implies conformational rearrangement for assembly or disassembly of these proteins and the complexes they form, thus

requiring chaperone activity to proceed. By helping these proteins to change the conformation, or refolding the damaged ones, chaperones allow the terminal to stay efficient for prolonged period and properly respond to stimuli. This statement is most probably also valid for other cell types where regulated exocytosis takes place, like the endocrine and exocrine glands.

2.5. Exocrine secretory glands in the gastrointestinal tract

2.5.1. General aspects of food digestion

Upon feeding, food is taken into the mouth cavity, where it is mechanically processed. The secretion from the salivary glands (parotid, submandibular, sublingual and other small salivary glands), containing amylase, softens the food and initiates the chemical processing of the food, mainly the complex sugars. After passing through the oesophagus and the stomach, the processed food enters the small intestine, where the final steps of the enzymatic degradation take place. The exocrine pancreas, the biggest gland of the digestive system, is the most important gland for the alimentary digestion. It secretes its many enzymes into the duodenum (initial part of the small intestine). Pancreatic enzymes are then activated and degrade the food. If at any point the exocrine pancreas is obstructed in delivering its enzymes to the duodenum, the food cannot be fully utilized, which at the end causes inability to gain weight.

2.5.2. Histology and physiology of major exocrine glands in the digestive tract

2.5.2.1. Pancreas

The exocrine pancreas is a secretory gland of epithelial origin with cells organized in acini. The acinar cells are polarized cells with clearly distinguishable larger baso-lateral pole, and a smaller apical pole. In an acinus, all of the cells are oriented with the apical pole towards the lumen of the acinus (Figure 2).

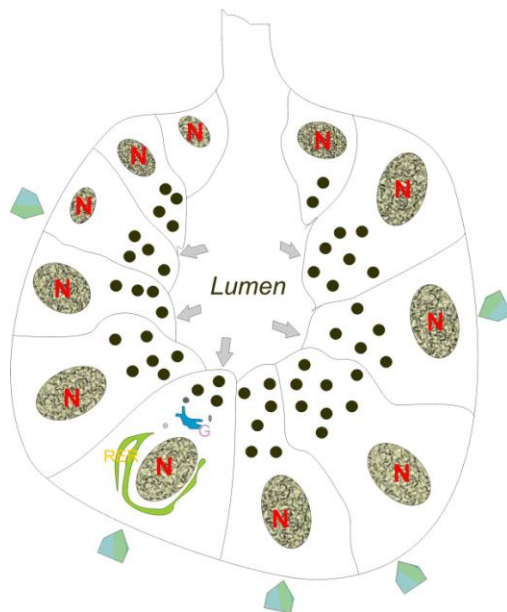


Figure 2: Schematic representation of pancreatic exocrine acinus (applicable also for parotid and submandibular glands)

In this simplified diagram a pancreatic acinus is presented, consisting of many acinar cells with different sizes. Their basal pole is oriented outwards (light blue arrowheads) and the apical pole (grey arrows) is oriented towards the lumen of the acinus. Secretory products (zymogens) are synthesized in the rough endoplasmic reticulum (RER, green colour) and transferred to the Golgi network (G, blue colour). There the zymogens are packed in the zymogen granules (black circles) and destined for exocytosis into the lumen of the acinus (Palade 1975; Cook et al. 1996).

The secretory products of the acinar cells are packed in the zymogen granules and upon stimulation, the zymogens are secreted into the lumen of the acinus. The actual membrane fusion of zymogen granules with the apical plasma membrane is believed

to be mediated by SNARE proteins in a manner similar to other membrane fusion events (for review, see Gaisano 2000; Williams 2006). Different members of the SNARE family have been identified in the pancreatic acinar cells. (Braun et al. 1994; Gaisano et al. 1996; Gaisano et al. 1997; Hansen et al. 1999; Wang et al. 2004; for review, see Gaisano 2000; Williams 2006). Different combinations of these SNAREs are responsible for different events of membrane fusion- apical exocytosis, granule-granule fusion, baso-lateral exocytosis and lysosome-granule fusion (reviewed in Gaisano 2000; Williams 2001; Williams 2006; Cosen-Binker and Gaisano 2007), enabling specificity of the fusion process.

2.5.2.2. Parotid gland

The parotid gland is a salivary gland, originating from the epithelia. Similar to the exocrine pancreas, it is exclusively serous gland with its cells organized in acini (Fig 2). The cells are secreting several hydrolytical enzymes which are responsible for the initial digestion of the food in the mouth cavity. Similar to the pancreas, the enzymes precursors are densely packed in zymogen granules and released into the lumen of the acinus upon stimulation (Stevens and Lowe 1992). It is suggested that, similar to other types of tissues, exocytosis in parotid acinar cells is mediated via the SNARE proteins. There are several members of the SNARE proteins already identified in the parotid cells (Imai et al. 2001; Imai et al. 2003; Wang et al. 2007).

2.5.2.3. Submandibular gland

The submandibular glands are typically mixed glands, containing both serous and mucous cells, with serous cells predominating. Cells are organized in acini (Figure 2), which sometimes contain both types of cells. The serous cells, similar to the exocrine pancreas and parotid gland, contain zymogen granules (Stevens and Lowe 1992).

So far, there is not any literature reference identifying SNARE isoforms in the submandibular glands.

2.6. Mast cells

Another cell type with secretory granules and regulated exocytosis is the mast cell. The mast cells are part of the immune system, and one of the defense mechanisms of the organism against foreign agents. Mast cells reside in support tissues, especially beneath epithelia, around blood vessels and serous cavities. They are characterized by the presence of secretory granules, containing histamine and other biologically active substances (Stevens and Lowe 1992). Upon stimulation, these vesicles are exocytosed (process often called “degranulation”) in the proximity of the target. It is well established that exocytosis in the mast cells is mediated via different members of the SNARE family of proteins (for review, see Blank et al. 2002; Logan et al. 2003; Pickett and Edwardson 2006).

2.7. Aim of the present study: CSP protein and the pancreas

It has been reported that CSP is present on the zymogen granules of the pancreatic acinar cells (Braun and Scheller 1995). In addition, CSP α KO mice are characterized, among else, with their inability to gain weight after P15.

The exocrine pancreas is very important gland for the digestion of the nutrients. The pancreatic acinar cells deliver their enzymes to the acinar lumen packed in zymogen granules via exocytosis, process mediated by members of the SNARE family proteins. Disturbance of exocytosis of secretory granules of digestive glands could

theoretically explain the postnatal developmental defect in weight gain of the CSP α KO mice.

This study aims at identifying ultrastructural changes in the pancreatic acinar cells, that could help understand the function of CSP α in the body and that could explain the inability to gain weight in the CSP α knockout mice.

In addition, exocrine glands of epithelial origin (parotid and submandibular) having zymogen granules are also examined, as well as peritoneal mast cells.

3. Materials and Methods

3.1. Chemicals and materials

<i>Product</i>		<i>Company</i>
100bp DNA-Leiter Roti® Mark		Carl Roth GmbH
10x PCR buffer		Sigma
10x PCR buffer Y		PeqLab
25% glutaraldehyde (EM grade)		Sigma
25mM MgCl ₂		PeqLab
Agarose		PeqLab
Azur II stain		Carl Roth GmbH
Borax		Carl Roth GmbH
Cacodylic acid		Carl Roth GmbH
Chloroform		ACROS Organics
Diethyl pyrocarbonate (DEPC)		Sigma
Disodium hydrogen phosphate		Carl Roth GmbH
Dithiothreitol (DTT)		Sigma
dNTPs PCR-grade		Carl Roth GmbH
EDTA		Carl Roth GmbH
EPON resin components	Embed-812, Dodecenyl Succinic Anhydride (DDSA), nadic methyl anhydride (NMA) and 2,4-tri(dimethylaminoethyl)phenol (DMP 30)	Electron Microscopy Sciences
Ethanol		Carl Roth GmbH

Ethidiumbromide	Carl Roth GmbH
Magnesium chloride	Carl Roth GmbH
Magnesium chloride hexahydrate	Carl Roth GmbH
Maleic acid	Sigma
Methylen blue	Carl Roth GmbH
OsO ₄	Chempur
Paraformaldehyde (PFA)	Sigma
peqGOLD Trifast reagent	PeqLab
PeqTaq polymerase	PeqLab
Phenol-chloroform	Sigma
Potassium chloride	Carl Roth GmbH
Potassium Hydrogen phosphate	Carl Roth GmbH
Potassium phosphate	Carl Roth GmbH
Proteinase K	Carl Roth GmbH
RedTaq Polymerase	Sigma
RNAlater	Quiagen
RNAlater-ICE	Ambion
Sodium chloride	Carl Roth GmbH
SuperScript™ III RNase H Kit	5x First Strand Buffer, 0,1M dithiothreitol [DTT] and Reverse Transcriptase enzyme [200U/μl] Quiagen
Tris acetate	Carl Roth GmbH
Uranyl acetate (UA)	Polysciences Inc.

Table 1: Chemicals and reagents used in the experimental procedures

<i>Product</i>	<i>Company</i>
Adjustable pipettes	Eppendorff
Agarose gel electrophoresis system	PeqLab
Autoclave	Tuttnauer Systec 5050ELCV
AxioCam MRm (Camera)	Zeiss
AxioVert 200M	Zeiss
Biofuge fresco	Heraeus
Biofuge primo R	Heraeus
Biofuge stratos	Heraeus
Chemidoc XRS system	BioRad
Diamond knife (4°)	Diatome AG
Freezer -80°C	Heraeus
Hot air oven	Heraeus
Leica UltraCut-S or –M ultratome	Leica Microsystems GmbH
Light microscope 4-40x	Olympus
Magnetic stirrer (Complete Set)	Neolab
MegaView IV CCD-camera	SIS GmbH
Multifuge S-R	Heraeus
Orbital Shaker	Edmund Bühler Labortechnik
PCR master cycler gradient	Eppendorff
pH meter	Inolab

Rugged rotator	Neolab
Sterile filtration device	Millipore
Tecnai Bio-Twin 12 electron microscope	FEI
Thermo mixer compact	Eppendorff
Vortex	VWR International
Weighing balance CP64	Sartorius

Table 2: Laboratory hardware equipment

<i>Software</i>	<i>Company</i>
Adobe Photoshop	Adobe Inc.
analySIS	SIS GmbH
AxioVision v. 4.x	Zeiss
ImageJ	National Institute of Health (NIH)
Microsoft Excel 2003 Professional	Microsoft
Quantity One package	BioRad Laboratories GmbH

Table 3: Software packages used in the processing of the digital data

3.2. Experimental animals

For studying the ultrastructural changes in the secretory glands of the digestive tract in CSP α KO mice, animals at postnatal day 17 (P17) were used. The mutant animals were previously generated (Fernandez-Chacon et al. 2004) and the animal line was kept by mating CSP α heterozygous parents. The animals were kept at the Department of Experimental Surgery at the Saarland University in constant light/dark 12h cycles. At P15-17 the entire respective litter was taken to the Institute of

Anatomy and Cell Biology, Department of Neuroanatomy where the dissection took place. The animals were dissected in the afternoon hours around 14:00h. The animals' tails were collected in separate microcentrifuge tubes, properly labelled, and used for DNA isolation and genotyping. The age of the animals was chosen at P15-17 because at this age the changes in the CSP α mice are initiating (see chapter 2.4).

3.3. Electron microscopy

3.3.1. Preparation of the solutions and buffers used for washing, fixing and embedding the tissues

<i>Buffer/Solution</i>	<i>Composition</i>
Phosphate-buffered saline (PBS)	40g Sodium Chloride, 1g Potassium Chloride, 7,2g Disodium hydrogen phosphate and 1,2 g Potassium phosphate dissolved in 1000ml distilled water.
4% PFA in PBS	4g PFA (paraformaldehyde) dissolved in 100ml PBS with heating to 60°C till the liquid becomes transparent, cooled to room temperature (RT) and then stored at 4°C
1% PFA in PBS	1:4 dilution of 4% PFA stock solution in PBS, always fresh prepared and stored at 4°C
2,5% glutaraldehyde in 1% PFA in PBS	1:10 dilution of 25% glutaraldehyde 1% PFA in PBS, always fresh prepared and kept at 4°C until use
Cacodylate buffer pH 7,4 200mM	42,8g cacodylic acid dissolved in 1000ml Millipore water, pH set to 7,4 and kept at 4°C until use

Cacodylate buffer pH 7,4 100mM	21,4g cacodylic acid dissolved in 1000ml Millipore water, pH set to 7,4 and kept at 4°C until use
0,05M maleate buffer pH 5,0	5,53g maleic acid dissolved in 1000ml Aqua dest, pH set to 5,0 and kept at 4°C until use
4% OsO ₄	1g OsO ₄ dissolved in 25ml Millipore water in dark bottle in cold room with constant shaking for ~3 days. The solution aliquoted in 1ml aliquots and stored at -20°C until use.
2% OsO ₄	1:1 dilution of 4% OsO ₄ with 200mM cacodylate buffer pH 7,4 prior to use.
2% uranyl acetate (UA) for block-contrasting	2g UA dissolved in 100ml 0,05mol maleate buffer pH 5,0 in a light-protected beaker. Prior to use, solution filtered through 0,2µm filter.
2% uranyl acetate (UA) for section-contrasting	2g of uranyl acetate dissolved in 100ml Millipore water in a light-protected beaker, filtered through 0,2µm filter and stored at 4°C until further use
EPON-mixture	26g EPON-812, 11g DDSA, 16g NMA and 0,4g DMP30 weighed in a 50ml falcon tube, shaken vigorously till the mixture gets orange-reddish, always fresh prepared or used within 2 days when stored at room temperature.

Table 4: Solutions and buffers (and their composition) used for washing, fixing and embedding the tissues

Safety note: the OsO₄ waste always collected in separate plastic or glass containers, gathered in special plastic container and removed from the lab by authorized personnel.

Safety note: the uranyl acetate waste always collected in separate plastic or glass containers, gathered in dark glass bottle and removed from the lab by authorized personnel.

Safety note: EPON-mixture waste was collected in separate plastic containers, polymerized at 60°C for at least 24 hours and then discarded.

3.3.2. Preparation of Richardson Blue stain

Solution A: 0,5g Azur II stain were dissolved in 50ml Aqua dest.

Solution B: 0,5g methylen blue and 0,5g borax were dissolved in 50ml Aqua dest.

Richardson Blue stain was prepared by mixing the two solutions in equal parts, mixing them on the shaker for ~1h and then filtering it trough filter paper to remove undissolved particles or precipitates. The stain solution was then kept at RT.

3.3.3. Organs harvesting, fixing and embedding for electron microscopy

3.3.3.1. Organs harvesting and protein fixing

A. Dissection of pancreas, gut, adrenal glands, salivary glands, cerebellum and pituitary gland

The animals were anesthetized with diethyl ether and kept under constant anaesthesia during the procedure. After opening the thorax, big venous vessel (V. cava sup. or inf.) was cut open and the animals were perfused trough the left ventricle first with ~4ml of PBS, followed by ~4ml of 2,5% glutaraldehyde in 1% PFA in PBS, applied manually with moderate pressure using 2,5ml syringe with 27G (gauge) needle. The organs of interest (pancreas, gut (jejunum), adrenal glands, parotid gland, submandibular gland, cerebellum, pituitary gland) were harvested and

immediately transferred to scintillation vials containing ~3ml of fixative (2,5% glutaraldehyde in 1% PFA in PBS). The organs were fixed overnight, at 4°C.

2,5% glutaraldehyde in 1% PFA in PBS fixes the proteins. The rest of the tissues processing is described in the section 3.3.3.2.

B. Collecting mast cells by peritoneal lavage

The mast cells were collected as described in (Ribeiro et al. 2000), with some modifications. Namely, the animals were anaesthetized with diethyl-ether and kept under mild anaesthesia. The abdominal skin was gently removed, avoiding any damage to the abdominal muscles and peritoneum. About 3ml of cold PBS were injected with 27G needle into the abdominal cavity and the abdomen was gently massaged for 1-2 min. With another needle the liquid was absorbed, transferred to microcentrifuge tube and the cells were pelleted for 5min, 5000rpm, RT. After that they were fixed with 2,5% glutaraldehyde in 1% PFA in PBS overnight, at 4°C, and then processed as in 3.3.3.2. From time to time during the processing, the cells were pelleted down at 5000rpm, 1-2min, at 4°C.

3.3.3.2. Embedding for electron microscopy

The procedure for conventional electron microscopy consists of several consecutive steps:

- A. Fixing of the proteins: it is the initial step of fixing, described in 3.3.3.1.

- B. Fixing of the lipids:
 - Washing in PBS, 3x 10min, 4°C.
 - Washing in 100mM cacodylate buffer pH 7,5, 3x 10min, 4°C.

- Fixing with 2% OsO₄ in 100mM cacodylate buffer pH 7,5, 1h, 4°C.
- Washing in 100mM cacodylate buffer pH 7,5, 3x10 min, 4°C.
- Washing in Aqua dest, 3x 10min, 4°C.

C. Contrasting of the proteins

- Washing in 0,05M maleate buffer pH 4,5, 3x 15min, 4°C.
- Block-contrasting of the proteins with 2% uranyl acetate in 0,05M maleate buffer pH 4,5, 3 h, 4°C.
- Washing in 0,05M maleate buffer pH 4,5 3x 15min, 4°C.
- Washing in Aqua dest. 3x 10min, 4°C.

D. Dehydration of the specimen

- Initial partial dehydration in increasing ethyl-alcohol concentrations (30%, 50% and 70%), 30min. each, at 4°C.
- Another partial dehydration in increasing ethyl-alcohol concentrations (80%, 90% and 2x 99%), 30 min. each, at room temperature.
- Final dehydration in propylenoxyde for 30min. at room temperature, under fume hood.

E. Infiltration of the samples with Epoxy resin

- Initial infiltration with Epon: propylenoxyde mixture (volume ratio 1:3, total volume per vial 6-7ml), overnight, under the fume hood, RT and opened vials. Overnight infiltration ensures evaporation of the propylenoxyde and good infiltration of the specimen with the resin.

- Infiltrating with pure Epon (~3ml per vial), 5h to overnight, at room temperature. In the meantime, samples were kept under vacuum for 1h to ensure complete removal of air.
- Second infiltration with pure Epon (~3ml per vial), 3-5h at room temperature.
- Transferring the samples into labelled block moulds and application of final Epon mixture (~0,5ml per specimen).
- Polymerization of the resin at 60°C for at least 36h.

3.3.4. Trimming and cutting

After the polymerization, the blocks' front surface was trimmed to a trapezoid form with up to 3mm width and up to 5mm height and was polished with self-made glass knives. For histological identification, semi-thin (500nm thick) sections were cut, heat-fixed to glass slides at 80°C, dyed with Richardson-Blue and observed with Olympus light microscope, 4-40x objective magnification. The ultra-thin sections (60-70nm thick, silver to silver-gray colour on the refraction chart) were cut with diamond knife (4° angle) with water-bath (Table 2), stretched with chloroform vapors, collected on copper or nickel mesh grids and stored in grid storage boxes until further use. The cutting of the semi and ultra-thin sections was performed on Leica UltraCut-S or -M ultratome (Table 2).

3.3.5. Section-contrasting

The collected ultra-thin sections were section-contrasted by immersing the copper or nickel mesh grids into 70µl drop of 2% uranyl acetate in Millipore water for 25 min. RT, in dark. Then they were washed 5-6x 5min. in Millipore water, air-dried and stored in the grid-storage boxes.

3.3.6. Analysis by transmission electron microscopy

The section-contrasted ultra-thin sections were observed under Tecnai Bio-Twin 12 electron microscope (Table 2) at 100 kV accelerating voltage and 3-8 μ A emission current. The images were taken by MegaView IV CCD-camera, which was controlled by analySIS software package (Table 3). The contrast of the images was corrected using Adobe Photoshop or ImageJ (Table 3).

3.3.7. Morphometric and statistical analysis of data

Morphometric analysis was performed with analySIS software package. The results were collected and imported in Microsoft Excel sheets (Table 3), where the statistical analysis was performed, using unpaired Student's T-test. The value of $p < 0,05$ was taken as significant.

3.4. RNA extraction and purification

3.4.1. Parotid gland

The parotid gland was dissected immediately after the death of the animal. It was immediately homogenized in 300 μ l of peqGOLD Trifast reagent with teflon homogenizer and the homogenate was transferred to a clean sterile 1,5ml microcentrifuge tube in which the Trifast reagent was filled up to 1ml. 200 μ l of chloroform was added and the whole suspension was vortexed for 15 seconds. After 10 minutes incubation at room temperature, it was centrifuged at 13000rpm, 10 minutes, 4°C, which separated the fluid in three phases: the upper fluid clear phase containing RNA, thick inter-phase containing proteins, and a fluid and more viscous lower phase which contains DNA and proteins. About 400 μ l of the upper phase was carefully transferred to new microcentrifuge tube and 1 ml of isopropranol was added.

After 45 minutes incubation at -20°C, it was centrifuged at 13000rpm, 15 min. 4°C, the supernatant was discarded and the pellet was washed in 500µl 75% ethanol with brief vortexing. Then it was centrifuged again at 13000rpm, 10 minutes, 4°C, the supernatant was discarded, the pellet was air-dried under hood for 20 minutes and resuspended in 40µl of RNase-free DEPC-treated water. After incubation at 55°C for 5 minutes, the tube was transferred to ice for 2 minutes and the optical density (OD) at 260 and 280 nm, the concentration in µg/ml and the OD_{260/280} was measured. Finally, the tube with the RNA was stored at -80°C until further experiments.

3.4.2. Mast cells

The BMMC were kind gift from Prof. Marc Freichel from the Department of Pharmacology and Toxicology, University of Saarland, Homburg (Vennekens et al. 2007). The cell pellet provided contained 10×10^{10} cells, which were resuspended in 4ml of the peqGOLD Trifast reagent, divided into four equal parts and processed under the same protocol as for the parotid gland (3.4.1).

3.4.3. Pancreas

For RNA isolation, pancreatic tissue was processed in several ways.

1. After dissecting the tissue from the sacrificed animal, it was homogenized (the whole organ or just part of it) in 500µl of peqGOLD Trifast reagent;
2. Immediately incubated in 1ml of RNAlater stabilization reagent, stored at -20°C until homogenization or homogenized immediately as previously described (3.4.1);
3. Immediately incubated in pre-chilled at -80°C RNAlater-ICE and stored at -20°C overnight;

4. Immediately pulverized in liquid N₂ using ceramic mortar and pestle (pre-chilled on ice) and then resuspending the pulver in 1 ml of the peqGOLD reagent.

For each of these methods of homogenizing and stabilizing the tissue, it was processed under the same protocol as described for the parotid gland (3.4.1).

3.4.4. Testis

The testes were dissected from the male animals, homogenized and processed in same way as the parotid gland (see 3.4.1).

3.5. Reverse transcriptase polymerase chain reaction (RT-PCR)

RT-PCR experiments were performed using the following protocol:

3.5.1. Reverse transcription

In a 50µl PCR tube the reagents shown in Table 5 were added.

<i>Reagent</i>	<i>Volume (in µl)</i>
H ₂ O sterile	9
10mM dNTP	1
oligo-dT primer (TTTTTTTTTTTTTTTTTTTT, 10ng)	1
total RNA (500 -1500ng)	2

Table 5: Composition of the PCR mixture used for reverse transcription

The mixture was incubated in an Eppendorf or PeqLab thermal cycler at 65°C, for 5 min. After keeping on ice for 2 min, to the mixture were added the reagents shown in Table 6.

<i>Reagent</i>	<i>Volume (in μl)</i>
5x First Strand Buffer	4
0,1M DTT	1
Reverse Transcriptase enzyme (200U/ μ l)	1
H ₂ O sterile	1

Table 6: Composition of the PCR mixture added at step 2 of the reverse transcription

This mixture was incubated in the same thermal cycler at 50°C for 1h, followed by 15 minutes at 72°C.

3.5.2. PCR

For each of the CSP isoforms, the mixture in Table 7 was prepared.

<i>Reagent</i>	<i>Volume (in μl)</i>
H ₂ O sterile	37
10x PCR buffer Y (PeqLab)	5
25mM MgCl ₂	2
10 mM dNTP	1
5' primer (10ng)	1
3' primer (10ng)	1
single strand DNA template (see 3.5.1)	2
PeqTaq Polymerase 1U/ μ l (PeqLab)	1

Table 7: Composition of the PCR mixture used for generating the second strand of the DNA

Primers used were as described in (Schmitz et al. 2006), and as shown in Table 8.

<i>CSP isoform</i>	<i>Type of primer</i>	<i>Primer sequence</i>
CSP α	5'	AGGCAGCGCTCACTCTCTAC
	3'	CCTCCCTTTCATCAGACTGC
CSP β	5'	AGCGGACTTTGTCAACATCA
	3'	CACGGGCCAACATTAAGAGT
CSP γ	5'	CTACAGGAACTGGCCTTGC
	3'	TCCTTACGAGGATGGGTGTC

Table 8: Primers and their sequences used for CSP RT-PCR

The conditions in the thermal cycler were as shown in Table 9.

<i>Step</i>	<i>Temperature</i>	<i>Time</i>	
Activation of the enzyme	95°C	5 min.	
Denaturation	95°C	45 sec.	35 cycles
Annealing	60°C	45 sec.	
Elongation	72°C	1 min.	
Final elongation	72°C	10 min.	

Table 9: Thermal cycler PCR conditions used in the CSP isotyping

After the end of the cycles, the products were cooled down to 4°C and then stored at -20°C until further use.

3.6. DNA extraction and purification for CSP genotyping

The DNA was extracted and purified according to these two protocols:

3.6.1. Phenol-chloroform extraction method

About 1-2mm of mouse tail probe was digested for 5h to overnight by incubating in 600µl SNET buffer (1% SDS, 400mM NaCl, 5mM Na₂-EDTA, 20mM Tris-HCl pH 8,0) and 2µl Proteinase K (20mg/ml) at 55°C, 800 rpm. After cooling to room temperature for 10min. 600µl of phenol-chloroform (lower phase) was added and the Eppendorf tubes were gently mixed. The centrifugation at 13000rpm, 10min, RT separated the fluids in 3 phases- upper one containing the DNA, an interphase containing proteins, and a lower fluid phase containing RNA. About 500µl of the upper phase was transferred to a new tube, and 1ml of isopropanol was added, mixed gently and then centrifuged again at 13000rpm, 10min, RT. Then the supernatant was discarded and the remaining pellet was washed in 500µl 70% ethanol by centrifuging at 13000rpm 10 minutes, RT. After discarding the supernatant, the pellet was air-dried under hood for 20-30 minutes, resuspended in 200-400µl 150mM Tris-HCl pH 8,5 and the concentration of the DNA was measured at 260 nm.

3.6.2. Two-step method for DNA extraction

A small piece of mouse tail probe (~2 mm long) was incubated in 50µl alkaline lysis reagent (25mM NaOH, 0,2mM EDTA) at 65°C, 1400rpm, for 30 min. followed by 15min. at 98°C, 1400rpm. After that it was transferred to ice and 50µl of neutralizing reagent (40mM Tris-HCl pH 4,8) were added. This was centrifuged at 13000rpm for 1-2min. and 50µl of the supernatant was transferred to new microcentrifuge tube, which was stored at -20°C till further use. This is a simple and fast method, but very “dirty” way to get genomic DNA. This method does not include precipitation of DNA with alcohol.

3.7. Genotyping for the wild type (WT) and knockout (KO) CSP allele

After measuring the concentration of the DNA at 260 nm, it was corrected to final concentration of 20ng/μl. The following mixtures for the PCR reaction were prepared either as master mixes for more samples or for single reaction (see Table 10 for WT and Table 11 for KO PCR reaction).

<i>Reagent</i>	<i>Volume (in μl)</i>
H ₂ O sterile	14
10x PCR buffer	2,5
25mM MgCl ₂	4,5
10mM dNTP	0,5
5' primer, 10ng (ACTGTTAAAGAGACTGTCATGAAAAAGG)	1
3' primer, 10ng (GGGGGAGGGAATGTGGGTGAGTGTAGTTAG)	1
RedTaq Polymerase (1U/μl)	0,5

Table 10: Master Mix of reagents used for the WT PCR reaction

<i>Reagent</i>	<i>Volume (in μl)</i>
H ₂ O sterile	18
10x PCR buffer	2,5
25mM MgCl ₂	1,5
10mM dNTP	0,5
5' primer, 10ng (TTGGCCCACCAGCTGGAGAGTAC)	0,5
3' primer, 10ng (GAGCGCGCGCGGCGGAGTTGTTGAC)	0,5
RedTaq Polymerase (1U/μl)	0,5

Table 11: Master Mix of reagents used for the KO PCR reaction

The conditions in the thermal cycler were as shown in Table 12.

<i>Step</i>	<i>Temperature</i>	<i>Time</i>	
Activation of the enzyme	95°C	5 min.	
Denaturation	95°C	45 sec.	40 cycles
Annealing	60°C	45 sec.	
Elongation	72°C	1 min.	
Final elongation	72°C	10 min.	

Table 12: Thermal cycler conditions used for the CSP genotyping

After the end of the cycles, the products were cooled down to 4°C and then stored at -20°C until further use. The expected size for the PCR product of the WT allele was about 600bp, and for the KO allele about 900bp.

3.8. Agarose gel electrophoresis

All of the PCR and RT-PCR products were cast in 1 or 1,5% agarose gel pre-treated with ethidium bromide, electrophoresed at 80-130mV in 1x TAE buffer and visualized under UV exposure in Chemidoc XRS system (*BioRad Laboratories GmbH, Germany*). The size of the respective DNA bands was compared against 100bp DNA ladder standards. Images were acquired using Quantity One package (Table 3) and stored in digital format.

4. Results

4.1. General remarks on EM quantifications

- For standardization of EM quantifications, only pancreatic acinar cells were considered for further analysis when the central lumen of the acinus was clearly visible. Additionally, only cells which contained a clearly visible nucleus were included for quantitative analysis. By this procedure, it is ensured that only cross-sections of cells from the central parts of the exocrine acinar cell, but not peripheral sections with untypical distribution of organelles were used for further analysis.

For each experiment at least 3 animals were analyzed.

- For standardizing the distribution of the granules in the cell, the following procedure was performed. First, the length of the cell was measured (line AB, Figure 3). The line was drawn from the middle point of the apical plasma membrane (point A, Figure 3), through the center of the nucleus (point C, Figure 3) to a point at the plasma membrane of the basal cell pole (point B, Figure 3). The granule closest to the basal pole was determined and a normal line from its center was put perpendicular to the AB line. The point of intersection of the two lines is point D. The relative length of the AD (line AB, Figure 3, expressed as percentage of the entire apico-basal cell length) is a parameter for quantitative determination of the granular distribution in the apico-basal direction.

These same criteria were applied when quantifying the distribution of the zymogen granules in the parotid and submandibular glands, too.

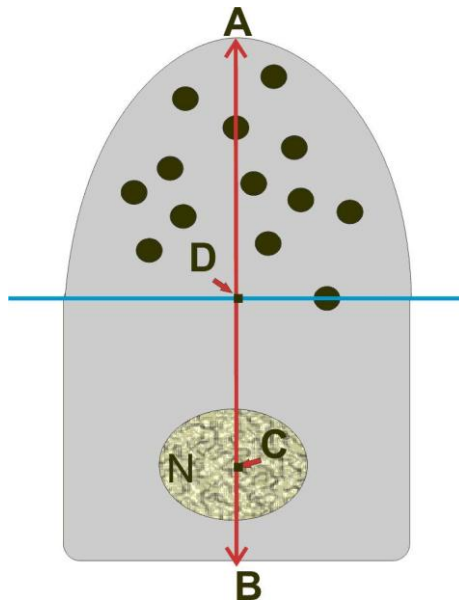


Figure 3: Schematic representation of an acinar cell and measuring the distribution of the granules in the cell

The granules occupy certain length of the cell (line AD), which can be presented as percentage of the cell length (X) using the formula $X=AD/AB$. A- center point of the apical pole of the cell, B-point at the basal pole, C- center point of the nucleus, N- nucleus, D- point of intersection between the two lines, black circles represent zymogen granules.

- The zymogen granules of the pancreas are, ideally, spherically shaped.

When processed, embedded and cut for EM, their cross-section is in the shape of a circle, or in some cases slight ellipse (see also Figure 4). In such cases, the largest diameter was used. For these quantifications, the polarity of the cells was not taken into account, meaning that granules from cells that didn't show an apical pole were also measured.

- The exocrine pancreatic acinar cell and its containing organelles are three-dimensional structures. Consequently, not all zymogen granules are found in the same plane. If only one single section is cut from the specimen, not every granule can be found in this plane, and for those that can be seen under the microscope, it isn't sure whether that is the actual size of the granule or not. As seen on Figure 4, one plane of a single section could display different granule sizes although the actual

size could be the same. On the other hand, a randomly chosen section could provide an underestimate of the actual granule size if the section is not in the very centre of the respective granule.

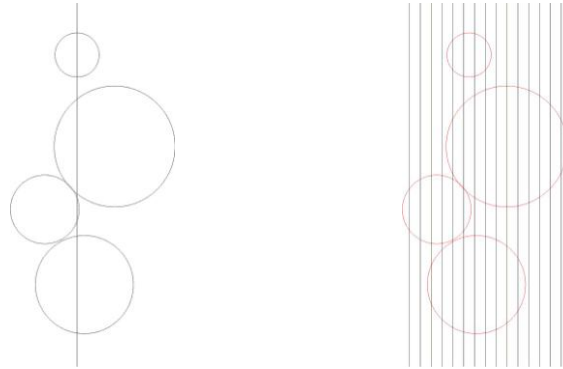


Figure 4: Scheme of single (left) and serial sectioning (right) of the zymogen granules

The circles represent the granules and the vertical lines represent the plane of cutting.

One option to get the actual value for the biggest diameter is to quantify large numbers of granules. Other option is to do serial sectioning of the specimen, collect every consecutive section and examine it under the EM (Figure 4 right-hand scheme). By these means, the changes in the diameter of the granules can be tracked in the consecutive sections and the maximal diameter can be estimated. Here, at least 50 serial sections from WT and KO samples were collected on Formvar- coated grids and examined in consecutive order. 50 different granules were chosen at one of the sections, and then identified in the next or previous sections, and the changes in their diameter were recorded. After finding the biggest diameter for every granule chosen, an average value was calculated.

4.2. Qualitative and quantitative transmission electron microscopy of exocrine pancreatic acinar cells in CSP α KO and WT control animals

The wild-type acinar exocrine cells of the pancreas displayed the well-known typical ultrastructural morphology (Figure 5 A, C, and E). The usually pyramidal-shaped acinar cells showed a polarized distribution of intracellular organelles: the basal pole was filled with large amount of rough endoplasmic reticulum (RER), whereas the zymogen granules were strongly concentrated in the apical portion of the cell. In contrast to this, the acinar exocrine cells of the pancreas in the CSP α KO mice showed a strongly different morphology when compared to the acinar cells from WT mice. Transmission electron microscopy analysis revealed that the pancreatic acinar cells from KO animals have more secretory granules, which are bigger and distributed widely in the cells (Figure 5 B, D and F). In the CSP α KO mice, normal looking cells were seen next to altered ones. In order to confirm the described structural alterations in the exocrine pancreatic acinar cell, quantitative electron microscopy analysis was performed and the results are explained in the following chapters.

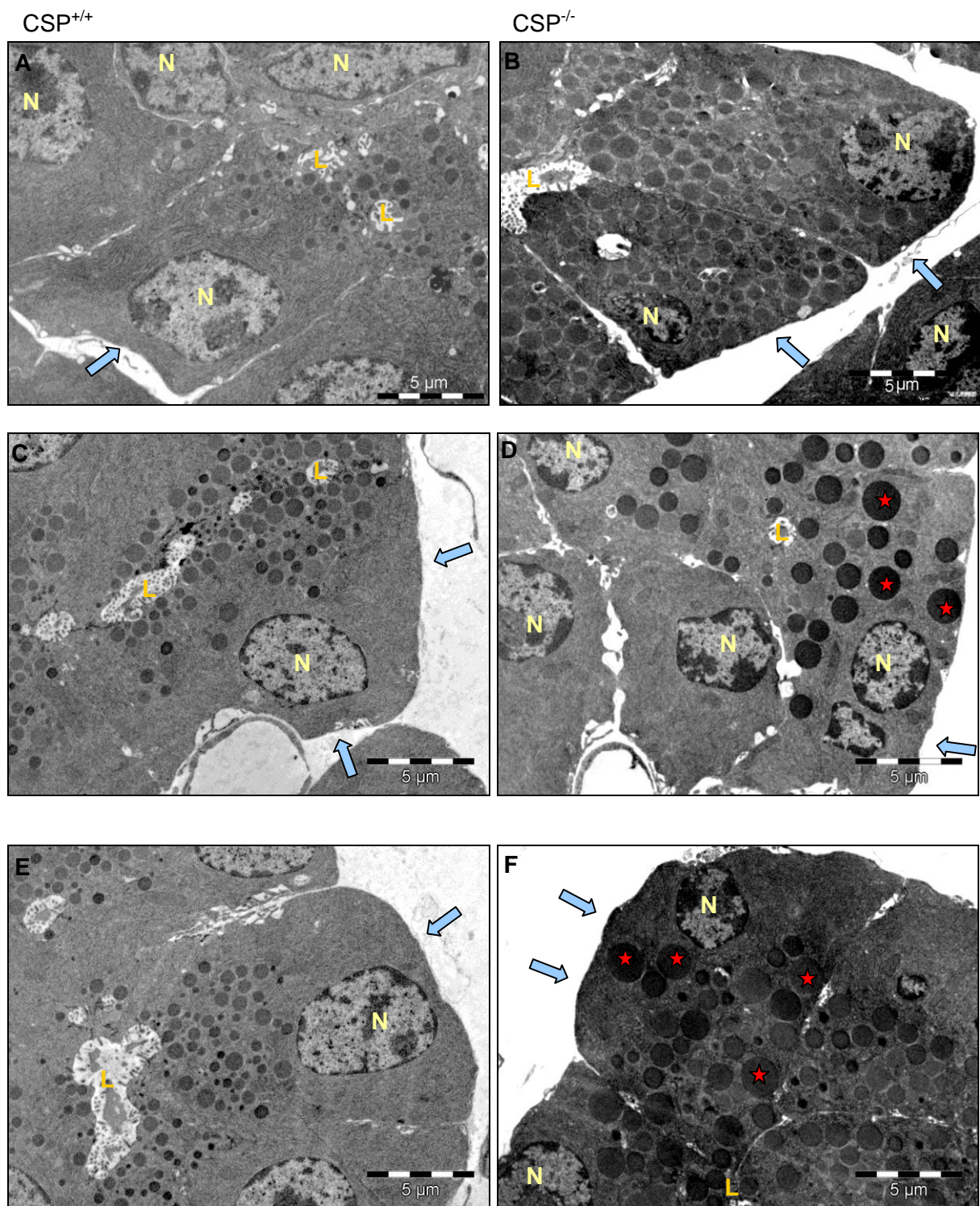


Figure 5: The phenotype of the exocrine pancreatic acinar cells in CSP wild-type and CSP knockout animals.

Ultra-thin sections of exocrine pancreatic acinar cells of CSP wild-type (A, C, E) and CSP knockout animals (B, D, F) were analyzed by transmission electron microscopy. Note the number and size of the granules in the CSP α KO pancreatic acinar cells in B), D) and F) as compared to the WT cells in A), C) and E). The cells in B) contain many granules which reach to the basal pole of the acinar cells; the cells in D) and F) have many granules with big diameter (red asterisks). N- nucleus, L- lumen, arrows point to the baso-lateral pole of the cell.

4.2.1. Number of zymogen granules per acinar cell

The average number of granules per cell section in the KO animals was 26.97 ± 1.08 , which is significantly higher than that of 21.46 ± 1.33 for the WT control mice ($p < 0.01$) (Figure 6 A). 45,74% of the cells from the KO animals have less than 20 zymogen granules per cross-section and thus fall into the category of “normal” cells (Figure 6 B, first 2 KO bars). The rest of the cells have higher number of zymogen granules, with some of them (22 cells, 9,87% of all cells from KO animals) having more than 50 granules. 63,39% of the 112 cells from the WT animals have less than 20 granules per cross-section. Only 5 cells (4,46% from all WT pancreatic acinar cells) have more than 50 zymogen granules per cross-section (Figure 6 B).

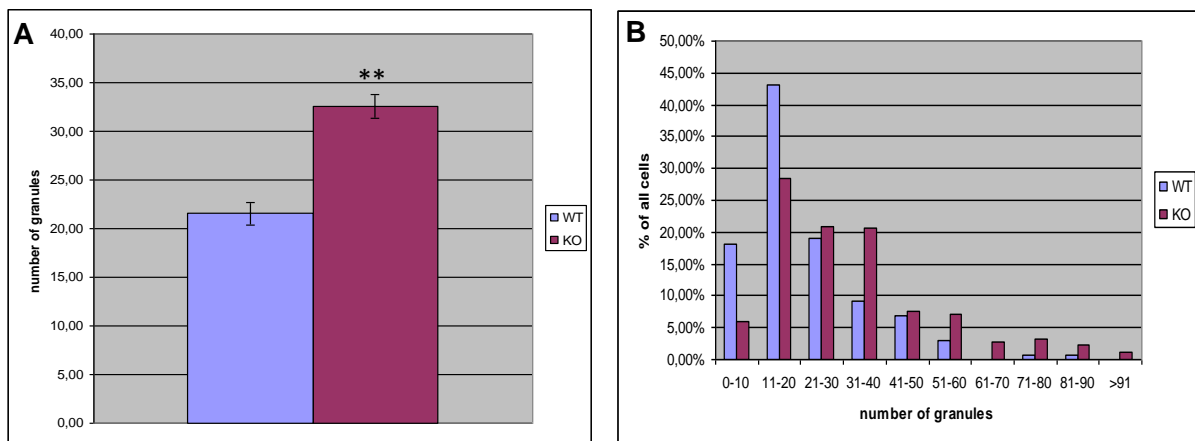


Figure 6: Granules number in pancreatic acinar cell

A) Number of granules per cell, $n = 156$ cells from 4 WT and 228 cells from 4 $CSP\alpha$ KO animals, ** - $p < 0.01$; B) normalized distribution of the cells according to the amount of granules.

4.2.2. Zymogen granules diameter

Quantitative electron microscopy suggested a strong increase in the diameter of the zymogen granules in pancreatic acinar cells from the $CSP\alpha$ knockout animals. The average diameter of the zymogen granules in KO cells is bigger than the average diameter of the zymogen granules from the WT cells. The respective means are

794,02± 4,28 nm for the granules from the KO cells and 590,90± 3,78nm for the granules from WT cells. This difference is statistically highly significant (Figure 7 A, p<0,001).

As shown in Figure 7 B), the diameter of granules from KO cell is shifted to the higher values. Most of the granules (1655, or 62,71% from all WT granules) in the WT cells have a diameter in the range of 400-800nm, with some of the granules reaching more than 1000nm in diameter (95 granules, or 3,60% of total). Most of the granules in CSP α KO cells (3199, or 62,09% of all KO granules) have their diameter in the range of 500-900nm. Some of granules have diameter below 500nm (521 granules or 10,11%). What is striking is the amount of granules (929, or 18,03%) that are present in the KO cells which have diameter much bigger than 1000 nm, in some cases reaching almost to 2000 nm (Figure 7 B), Figure 5).

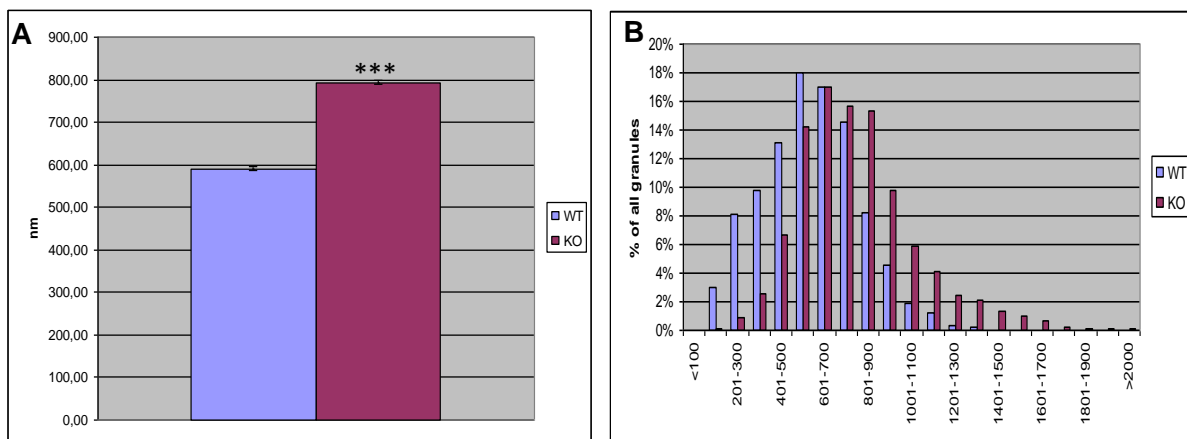


Figure 7: Zymogen granule diameter in pancreatic acinar cells

A) Average diameter of zymogen granules, n= 2639 granules from 4 WT mice and 5152 from 4 KO mice, bars are average± s.e.m, ***- p<0,001; B) normalized distribution of the granules in classes according to their diameter.

4.2.3. *Serial sections, average maximum diameter and average volume of the zymogen granules*

At least 50 serial sections from WT and KO samples were collected on Formvar-coated grids and examined in consecutive order to determine average maximum diameter and average volume as described above (chapter 4.1). 50 different granules were chosen at one of the sections, and then identified in the next or previous sections, and the changes in diameter were recorded. After finding the largest diameter for every analyzed granule, an average value was calculated (Figure 8 A). Once again, the diameter of granules in CSP α KO animals is bigger than in WT control animals. The average maximal diameter as measured by serial sectioning shows bigger values (for both WT and KO animals) than the average diameter previously measured (Figure 7). This larger value is expected because with the second method only the maximal diameter of granules was taken into account. In the previous quantifications shown in Figure 7 A), the diameter was measured in only one randomly picked plane in which the respective granule must not necessarily have its maximal diameter. With serial sectioning, the **maximal diameter** was always measured.

Using the value of the **average maximal diameter**, the average volume of the granules was calculated, according to the formula for the volume of a sphere: $V=4/3\pi r^3$. The average volume of granules from CSP α KO mice is $1,36\mu\text{m}^3 \pm 0,08$, which is significantly bigger than that of $0,51\mu\text{m}^3 \pm 0,02$ for the WT animals ($p < 0,001$).

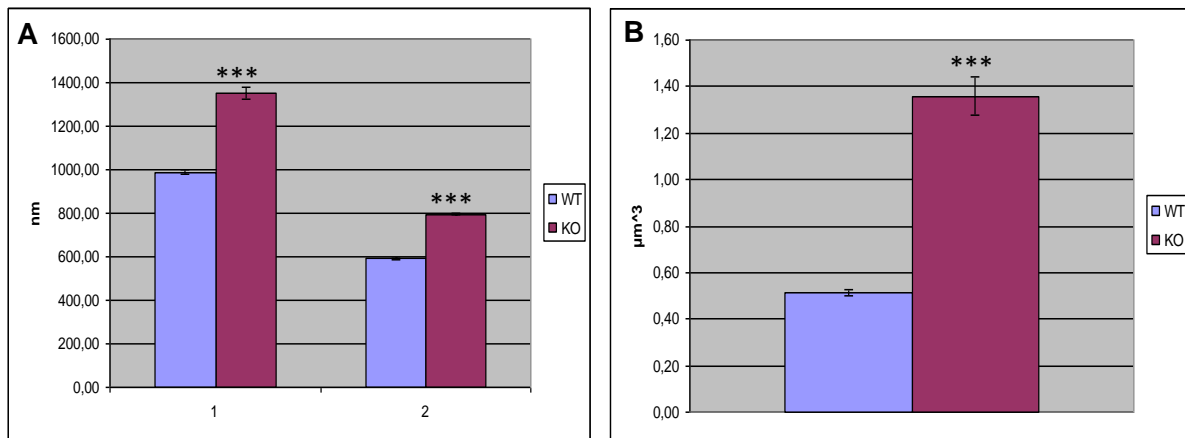


Figure 8: Diameter and volume of zymogen granules from serial sectioning

A) Average diameter of the pancreatic zymogen granules: 1- calculated from at least 50 serial sections; 2- calculated from normal cross-sections. B) Average volume of the zymogen granules in WT and KO pancreatic acinar cells, ***- $p < 0,001$.

4.2.4. Distribution of zymogen granules in exocrine pancreatic acinar cells

Figure 5 indicated that there are not only changes of size and number of secretory granules in $CSP\alpha$ KO mice, but also differences in the intracellular distribution of the granules.

Remarkably, in many KO cells, the zymogen granules were not only found in the apical pole, but also at the basal pole of the cell. Most of the times, these are the same cells that contain an increased number of zymogen granules that are bigger in size. Not all cells were altered though. There were cells (~42%) that looked comparable to the cells from the WT pancreas.

In an attempt to compare the distribution of the granule pool in the cells from the $CSP\alpha$ KO and their respective WT littermate controls, the following measurements were done. Object of quantification were only cells satisfying the criteria in 4.1.

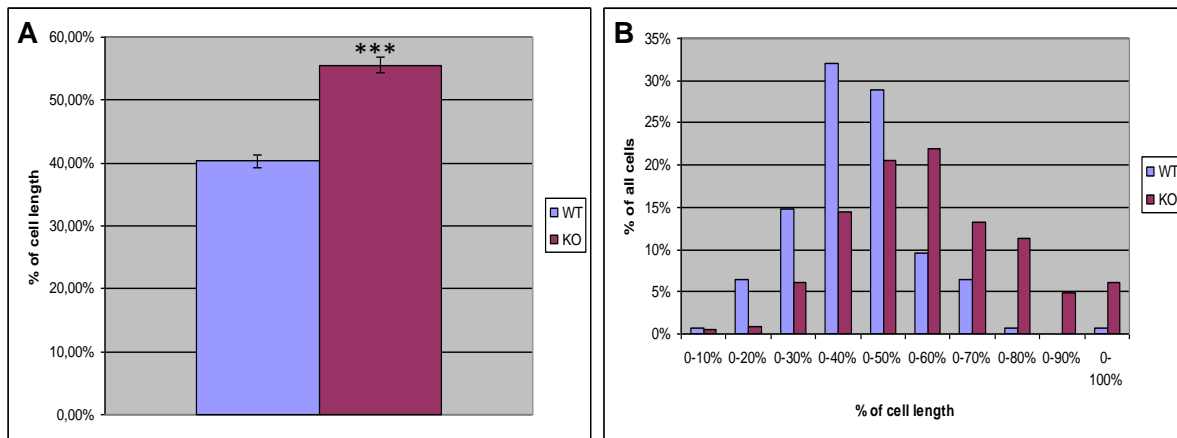


Figure 9: Distribution of the granules in the pancreatic acinar cells

A) Average distance of the granule pool from the apex of the cell, B) normalized distribution of the cells in classes; n=156 cells from 4 WT animals, 228 cells from 4 KO animals; ***- p<0,001.

The diagram in Figure 9 B) shows that there is difference in the distribution of the secretory granules in the acinar cell. In average, the zymogen granules are more widely distributed in the cell cytoplasm in the cells from the KO animals. Their distribution range comprises up to 55,53%± 1,25 of the cell length, which is significantly higher than that of 40,32%± 1,06 for the WT cells (p<0,001). Cells with differently distributed granules are found next to cells with normal phenotype (Figure 9 B). Most of the WT cell (129, or 82,69%) have their granules in up to 50% of the cell length, with only 27 or 17,31% of the cells having their granules widely distributed (in more than 50% of the cell length). In contrast to this, part of the KO acinar cells (97, or 42,54%) have their granules distributed in the first 50% of the cell length and the majority of the cells (132, or 57,46%) having their granules widely distributed (Figure 9 B).

4.3. Quantitative transmission electron microscopy of parotid acinar cells in CSP α

KO and WT control animals

I analyzed whether similar changes observed in the exocrine pancreas are also present in the parotid gland (Figure 10). The same parameters quantified for the exocrine pancreatic acinar cells were quantified for the acinar parotid cells, too.

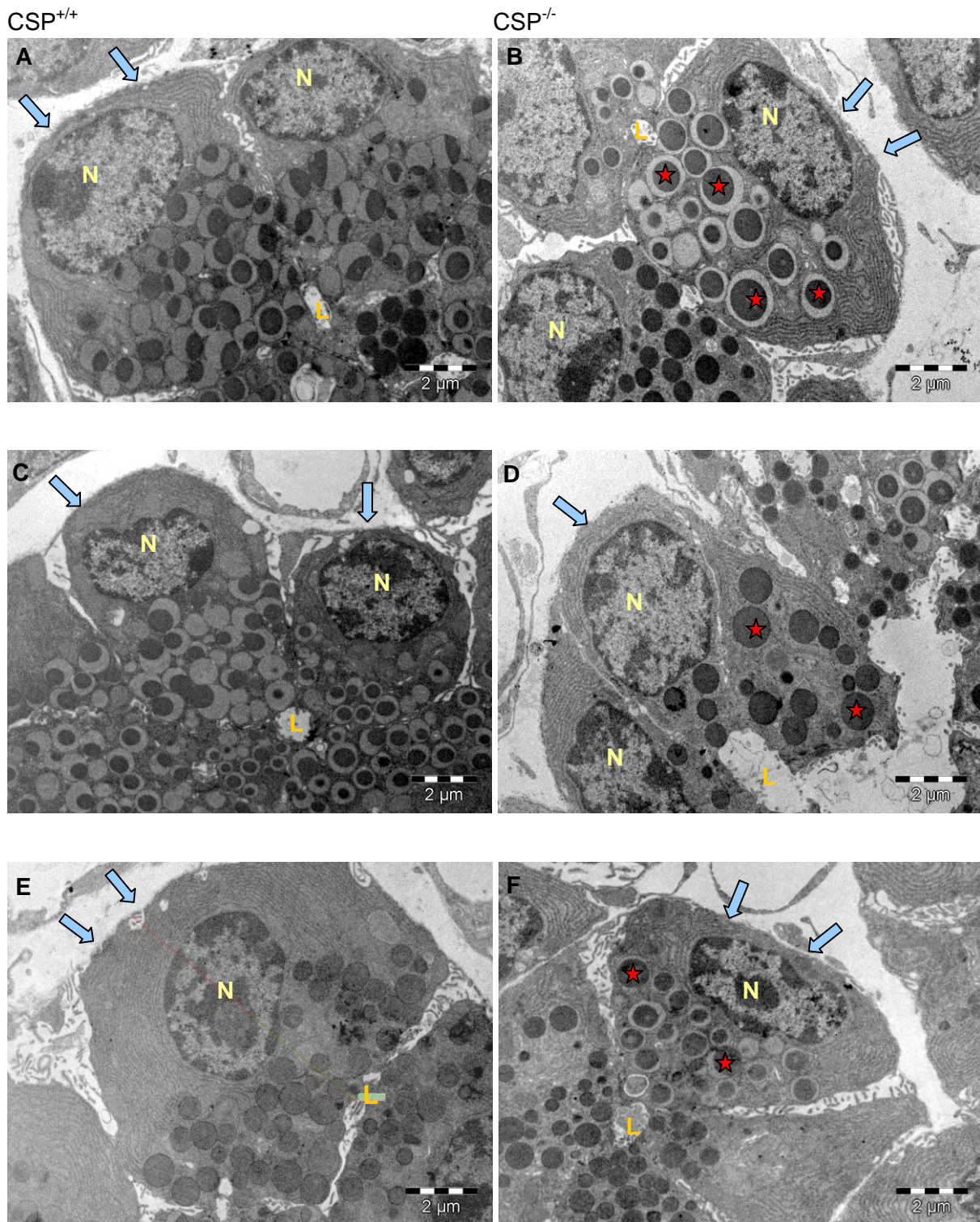


Figure 10: The morphology in the acinar cells of the parotid gland in CSP α KO and WT animals
 A), C) and E) cells from CSP α WT mice (CSP^{+/+}); B), D) and E) cells from CSP α KO mice (CSP^{-/-}).
 The cells from the mutant animals have granules with bigger diameter (red stars). The morphology of the zymogen granules with dense center and bright ring surrounding it is typical for the parotid glands.
 N- nucleus; L- acinar lumen; arrows- basolateral pole of the cells.

4.3.1. Zymogen granule diameter

Similar to the pancreatic acinar cells, the zymogen granules of the cells from parotid gland of the CSP α KO animals are bigger than the zymogen granules from the WT animals (Figure 10). Zymogen granules from the CSP α KO mice have average diameter of 803,94 \pm 4,93nm which is significantly bigger than that of 694,27 \pm 2,35nm in WT mice (Figure 11 A, p<0,001).

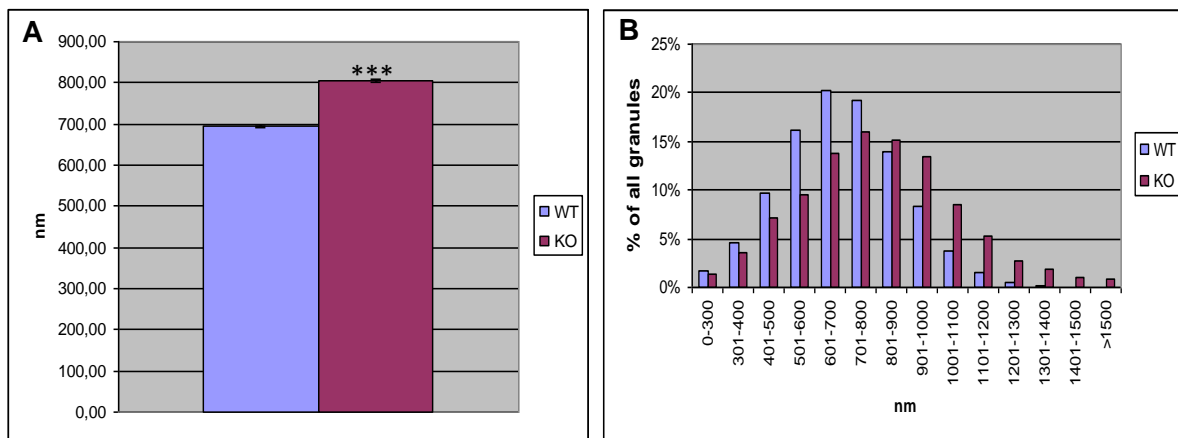


Figure 11: Zymogen granule diameter in the parotid acinar cells

A) Average zymogen granule diameter in WT and KO cells; n= 3469 zymogen granules from 3 animals for WT and n= 4312 granules from 3 animals for KO. Bars: average \pm s.e.m, ***- p<0,001; B) distribution of these granules in classes according to their diameter.

In addition, the overall distribution of the granules according to their diameter is shifted to the higher values (Figure 11 B), showing that the increased average diameter is not coming just from one or several sub-populations of the granules, but it is a systematic shift. As shown in Figure 11 B), the diameter of granules from KO cell is shifted to the higher values. Most of the granules (4799, or 69,66% from all WT granules) in the WT cells have a diameter in the range of 500-900nm, with some of the granules reaching more than 1000nm in diameter (422 granules, or 6,13% of total). Most of the granules in CSP α KO cells (2020, or 58,23% of all KO granules)

have their diameter in the range of 600-1000nm. Some of granules have diameter below 600nm (746 granules or 21,50%). Similar to the pancreatic acinar cells, there are a lot of granules (703, or 20,27%) that are present in the KO cells which have diameter much bigger than 1000 nm. The biggest granule measured in the KO cells had diameter of 1615,12nm.

4.3.2. Average granule number per acinar cell

Surprisingly, the average number of granules in the acinar cells of the parotid gland shows different characteristics than that observed in the pancreatic acinar cells. As shown in Figure 12 A), there is significant difference ($p < 0,001$) in the average granule number of the acinar cells of the parotid gland, but in contrast to the pancreas, exocrine cells from the wild-type animals' parotid gland have on average more granules ($18,69 \pm 0,59$) than the cells from the KO animals ($15,21 \pm 0,73$).

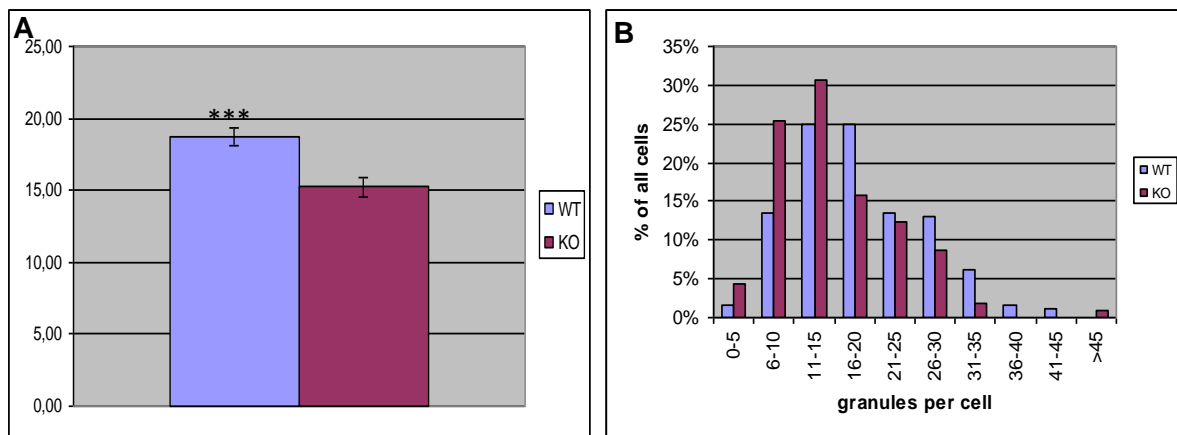


Figure 12: Granule number in the parotid acinar cells

A) Average granule number in the parotid acinar cells, WT n= 4 animals, 193 cells, KO n= 3 animals 114 cells, bars: average± s.e.m; ***- $p < 0,001$; B) normalized distribution of parotid acinar cells in classes according to their granule count.

The majority of the WT cells (176, or 91,16%) contain up to 30 granules, with the rest having up to 45 granules per cell. In contrast to this, 97,37% of the KO cells (or 111) have 30 or less granules, with 2 cells (1,75%) having 30-35 granules and only 1 (0,88%) having more than 45 granules (Figure 12 B).

4.3.3. Distribution of zymogen granules in parotid acinar cells

Quantifications of the distribution of secretory granules were done in same way as for the pancreas and as shown in Figure 9 A). Similar to the pancreas, the granules in the parotid cells in the KO animals are more widely distributed in the cell cytoplasm when compared with the cell from the WT animals (Figure 13 A). In the WT animals, the total granule pool reaches on average up to $47,73 \pm 0,94\%$ of the total length of the cell, while in the cells from the KO animals the total granule pool reaches up to $53,54 \pm 1,58\%$ of the length of the cell. This difference is significant ($p < 0,01$).

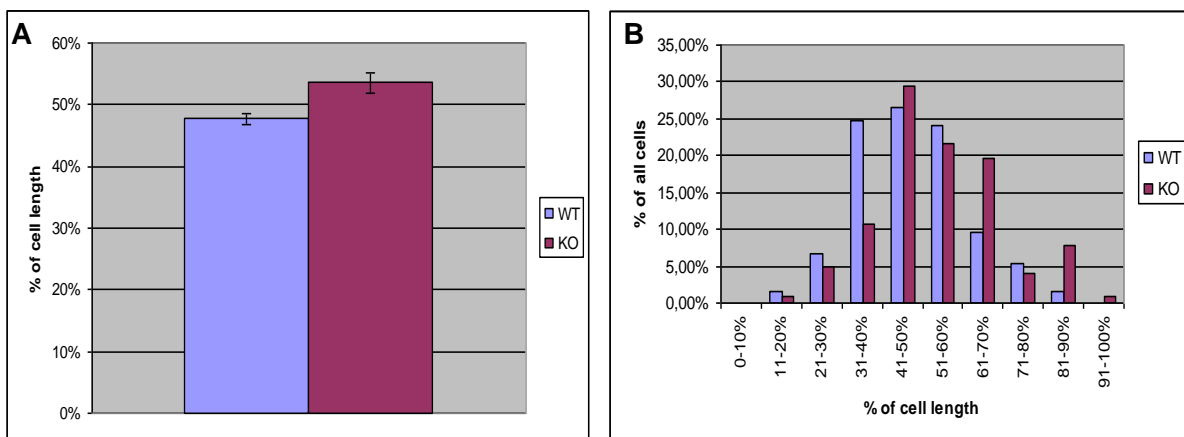


Figure 13: Quantification of distribution of zymogen granules in parotid acinar cells

A) Average distance of the granule pool from the apex of the cell, bars: average \pm s.e.m, n= 102 cells from 3 KO animals and 207 cells from 4 WT littermate controls; B) normalized distribution of parotid acinar cells in classes according to distribution of the granules in the cell.

Similar to the pancreatic acinar cells from the CSP α KO animals, the majority of the population are cells with widely distributed granules (55 cells, or 53,92%). Part of the KO parotid cells (47, or 46,08%) have their granules distributed in the first 50% of the cell length. Most of the WT cell (123, or 59,42%) have their granules in up to 50% of the cell length, with 84 or 40,58% of the cells having their granules widely distributed (in more than 50% of the cell length).

4.4. Quantitative transmission electron microscopy of submandibular serous acinar cells in CSP α KO and WT control animals

The serous exocrine cells in the submandibular gland from the CSP α KO animals showed a very strong morphological phenotype. As seen in Figure 14, many of the CSP α KO cells contain granules of very large size. Particularly striking is the heterogeneity of the granules shapes and forms. Higher magnifications micrographs of these granules suggest that their size and shape could result from inter-vesicular fusion (Figure 15, see also discussion).

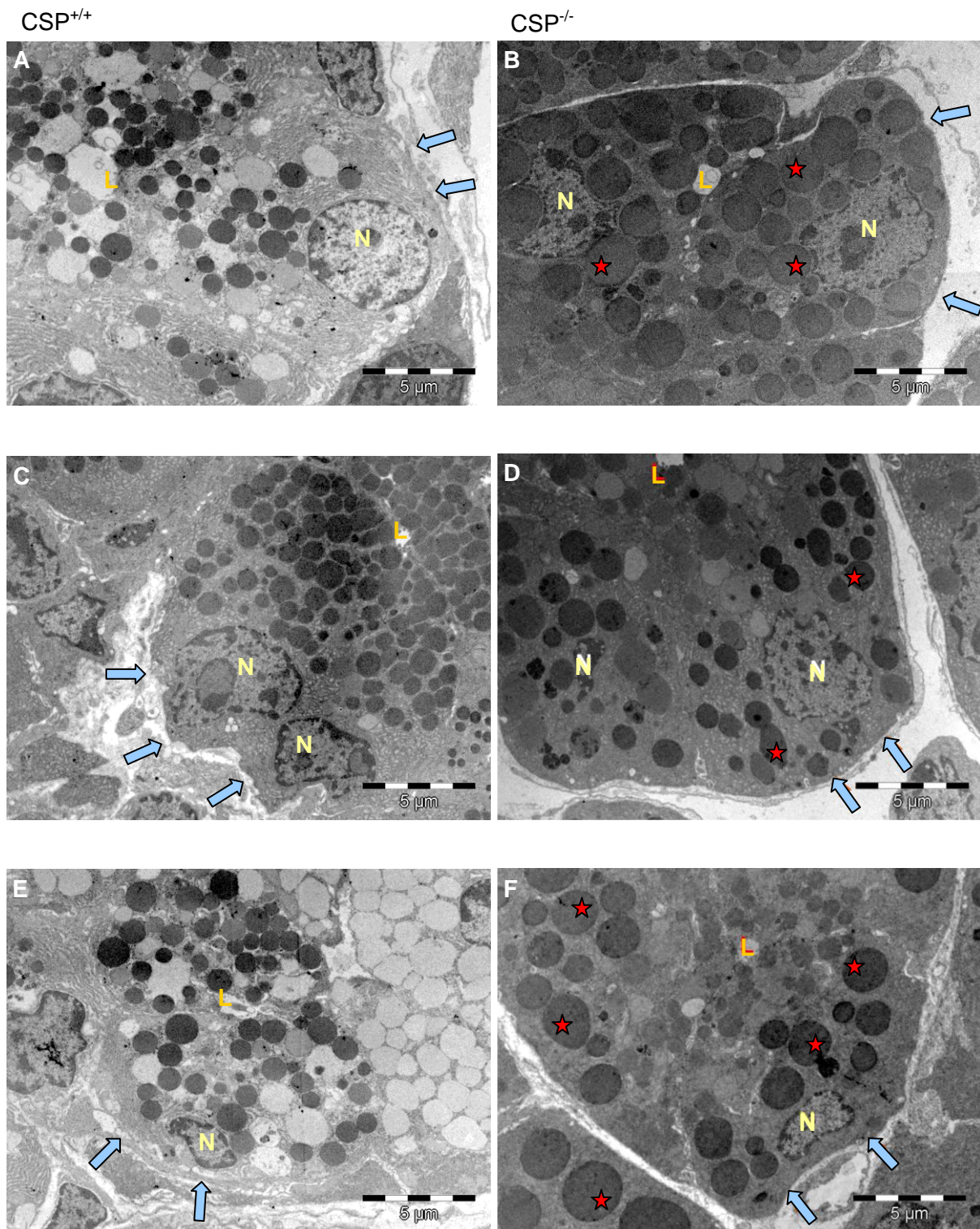


Figure 14: Morphology of the acinar cell from the submandibular gland of CSP wild-type (A, C, E) and CSP knockout (B, D, F) mice.

Many large zymogen granules (red asterisks) are seen in the cells from the CSP α KO animals (CSP $^{-/-}$; B, D, F). This kind of granules is not observed in the cells originating from the WT controls (CSP $^{+/+}$; A, C, E). N- nucleus, L- lumen, arrows point to the baso-lateral pole of the cells.

CSP^{-/-}

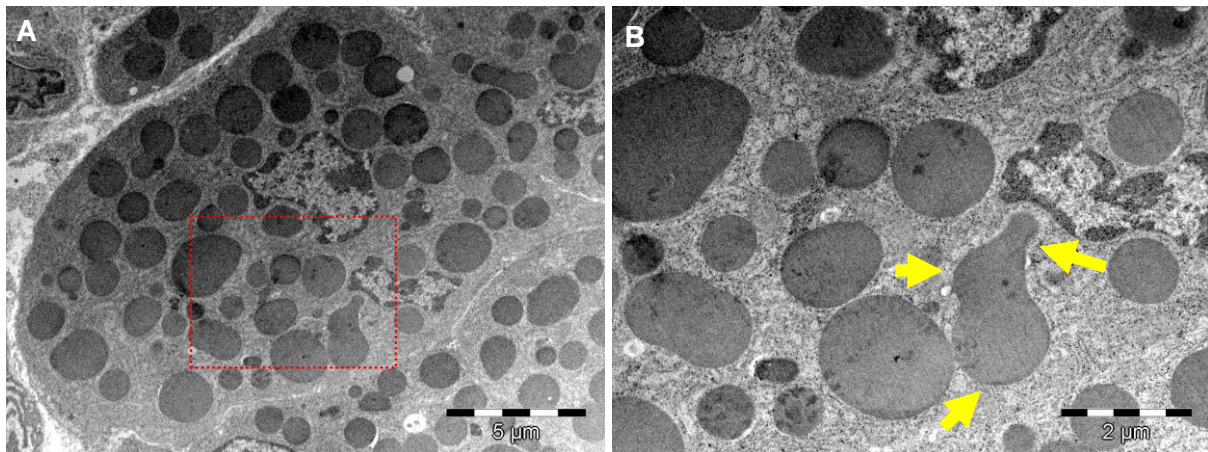


Figure 15: Some of the heteromorphous granules in the submandibular gland of CSP knockout animals at higher magnification

A) Overview of a submandibular serous acinar cell from CSP α KO mouse (CSP^{-/-}) containing many heterogeneously sized granules. The red rectangle surrounds an area shown at higher magnification in B). Yellow arrows point to possible separate granules fused together.

4.4.1. Zymogen granule diameter

Also for this exocrine gland, the size of the granules was measured. Some of the granules had spherical form, but some of the granules had very heterogeneous shapes. In such cases, the longest diameter was measured. When quantifying the diameter of the granules in the serous submandibular cells, the average granule diameter of the mutant animals is $1144,59 \pm 8,32$ nm and that of the wild-type littermate controls it is $844,30 \pm 5,01$ nm (Figure 16 A). This difference is highly significant ($p < 0,001$). When observing the normalized distribution of the granules in classes according to their diameter, one can see an enormous difference between the wild-type and mutant animals. In the WT animals, most of the granules (1778, or 65,58%) have their diameter in the range of 600-1100 nm (Figure 16 B). Only a small part (433, or 15,97%) of the WT granules are larger than 1100nm in diameter. WT granules having a diameter less than 600nm are in total 500, or 18,44%. In contrast

to this, only 1309 (or 42,01%) of the KO granules had diameter in the range from 600-1100nm. 1521 granules (or 48,81% of total) had diameter larger than 1100nm, with 8 granules (or 0,26%) having diameter larger than 3µm (Figure 16 B). The rest of the KO granules (286, or 9,18%) had diameter less than 600nm (Figure 16 B).

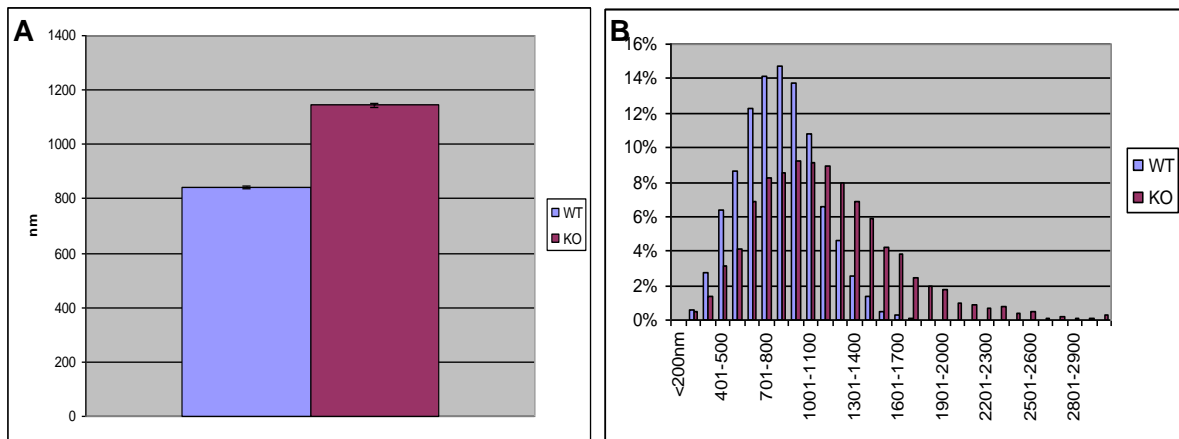


Figure 16: Zymogen granule diameter in the submandibular acinar cells

A) Average diameter of the zymogen granules, n=2711 granules from 3 WT animals and n=3116 granules from 3 KO animals, bars: average ± s.e.m, ***- p<0,001 B) distribution of these granules in classes according to their diameter.

4.4.2. Average granule number per acinar cell

Similar as in the pancreatic acinar cells, the mutant animals have more granules in their submandibular cells than the WT controls. On average, the acinar cells from the CSPα KO animals have 46,14±3,63 granules per cell, which is significantly higher than that of 29,42±1,83 granules from acinar cells of WT controls (Figure 17, p<0,001). Most of the WT cells (48, or 81,36%) have 40 or less granules per cell. The cells containing more than 41 granules are only 18,64% of the total amount of WT cells analyzed (Figure 17 B). In contrast to this, KO cells with less than 40 granules per cell section are 30 in total (or 52,63%). The rest of the cells have more than 40 granules per cell section (Figure 17 B).

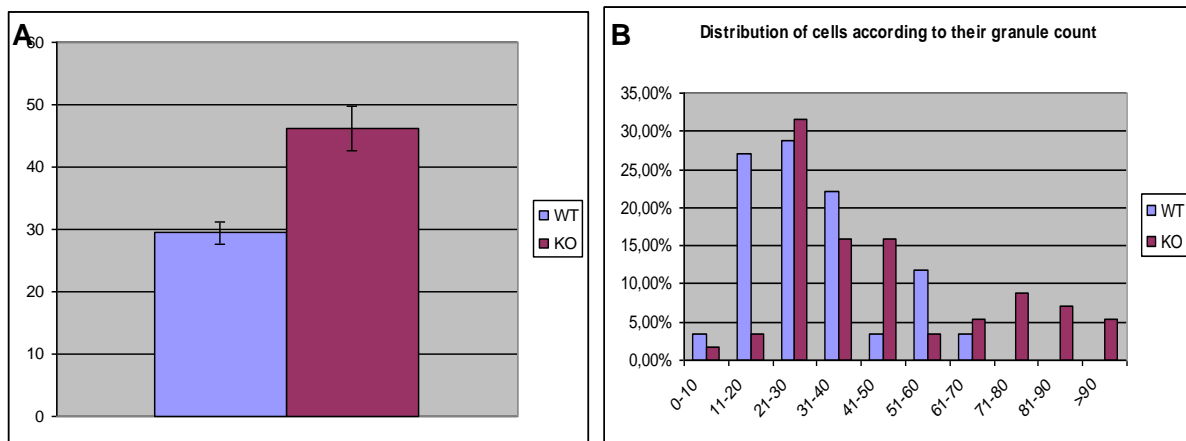


Figure 17: Zymogen granule number per acinar cell

A) Average number of granules per submandibular acinar cell, for the WT n=59 cells from 3 animals and for the KO n= 57 cells from 3 animals, bars: average \pm s.e.m; B) normalized distribution of the cells according to the number of granules.

4.4.3. Distribution of zymogen granules in submandibular serous cells

Similar to the pancreas and parotid gland, the zymogen granules in the submandibular serous cells from the CSP α KO animals are widely distributed in the cytoplasm of the cells (Figure 14). In average, the granules in the CSP α KO animals take up to 87,86 \pm 1,90% of the cell length, which is significantly higher than that of 61,14 \pm 1,94% for the WT cells (Figure 18 A), p<0,001). 6,78% of the WT cells have their granules in up to 50% of the cell length, with 28,81% of the cells having their granules widely distributed (within 91-100% of the cell length). In contrast to this, part of the CSP α KO submandibular acinar cells (1,75%) have their granules distributed in the first 50% of the cell length and the majority of the cells (61,48%) having their granules distributed throughout the entire cell (91-100% of cell length, Figure 18 B).

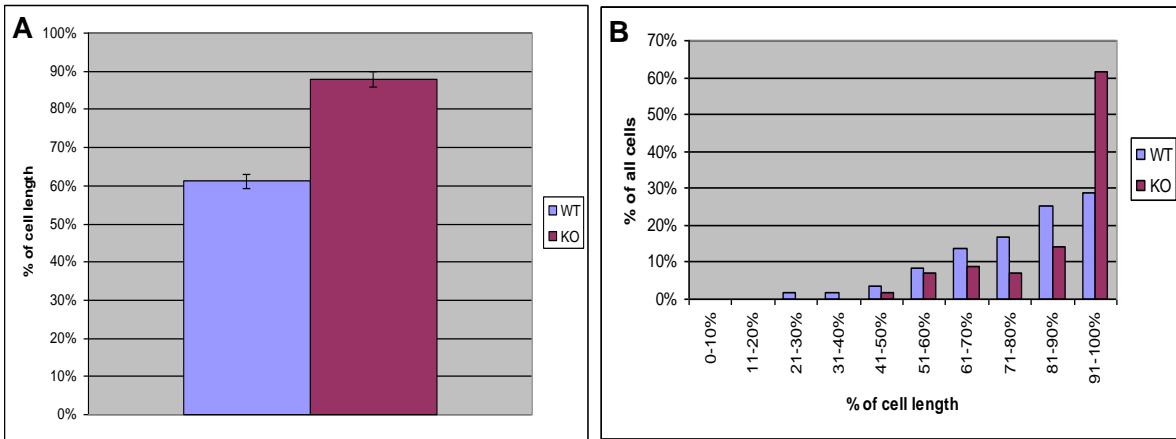


Figure 18: Distribution of the zymogen granules in the serous acinar cells of the submandibular gland

A) Average distance of the granule pool from the apex of the cell, bars: average \pm s.e.m, n=57 cells from 3 KO animals and 59 cells from 3 WT littermate controls; B) Normalized distribution of the cells according distance of the granule pool from the apex of the cell. Note the high percentage of the cells from the CSP α KO animals having their granules widely distributed (last KO bar, 91-100%).

4.5. Mast cells

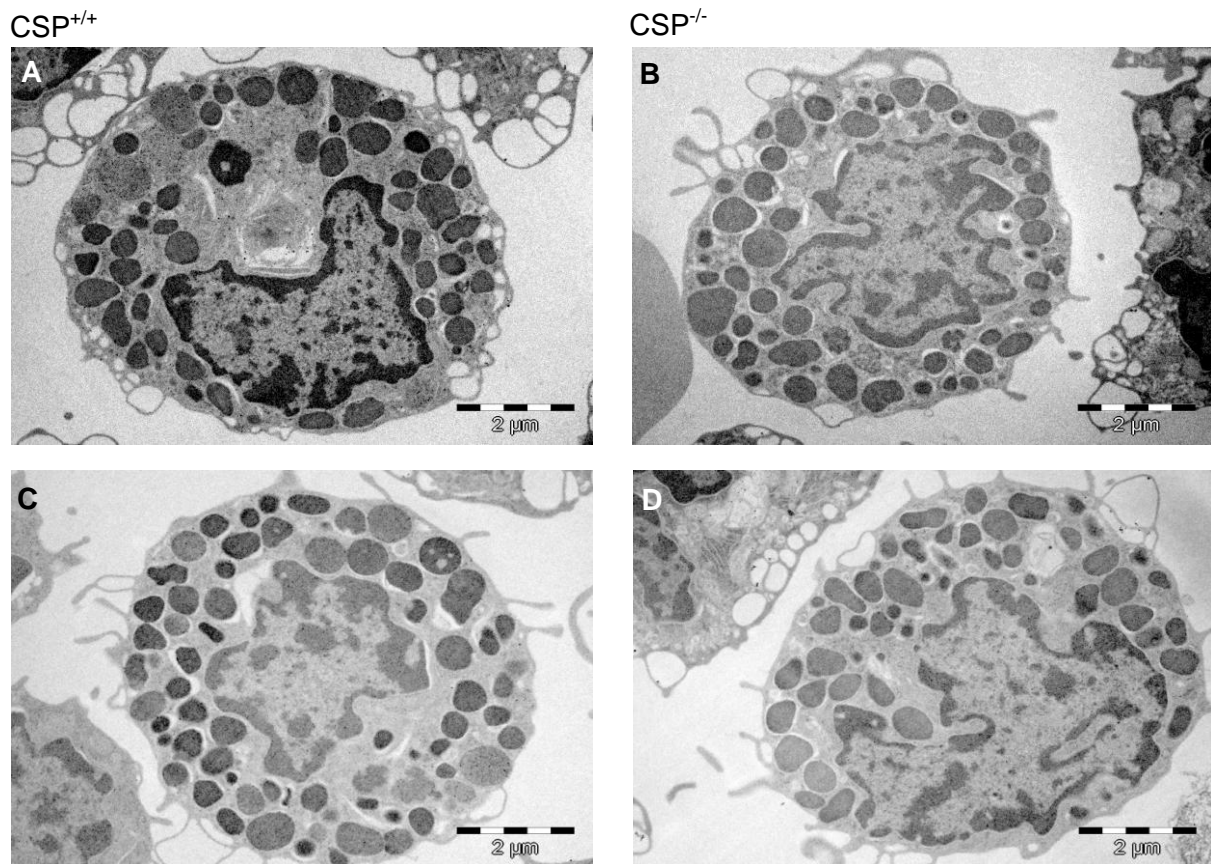


Figure 19: Peritoneal mast cells

No visible differences can be observed; the cells from the WT (CSP^{+/+}; A, C) and KO (CSP^{-/-}; B, D) animals look identical; N-nucleus, arrows point to secretory granules

When ultra-thin sections of the mast cells were observed under the EM, no obvious differences between the cells from the CSP α KO and WT animals could be seen (Figure 19). This lack of difference was confirmed by several quantifications. There were no differences in the cell size ($6,92\pm 0,89\mu\text{m}$ for the KO and $7,12\pm 0,15\mu\text{m}$ for the WT cells, measured as diameter and only for cells that had nicely visible nucleus, as seen in Figure 19). Also, no differences were found for number of granules per cell ($46,92\pm 1,47$ for the KO and $49,24\pm 1,65$ for the WT cells), or diameter of the granules ($546,88\pm 5,34\text{nm}$ for the WT and $547,53\pm 4,14\text{nm}$ for the KO animals, Figure 20 A). It

is worth noting that mast cells from only one CSP α KO mouse and two CSP α WT mice were processed and quantified. Therefore, these results have to be complemented by further analyses using more mice.

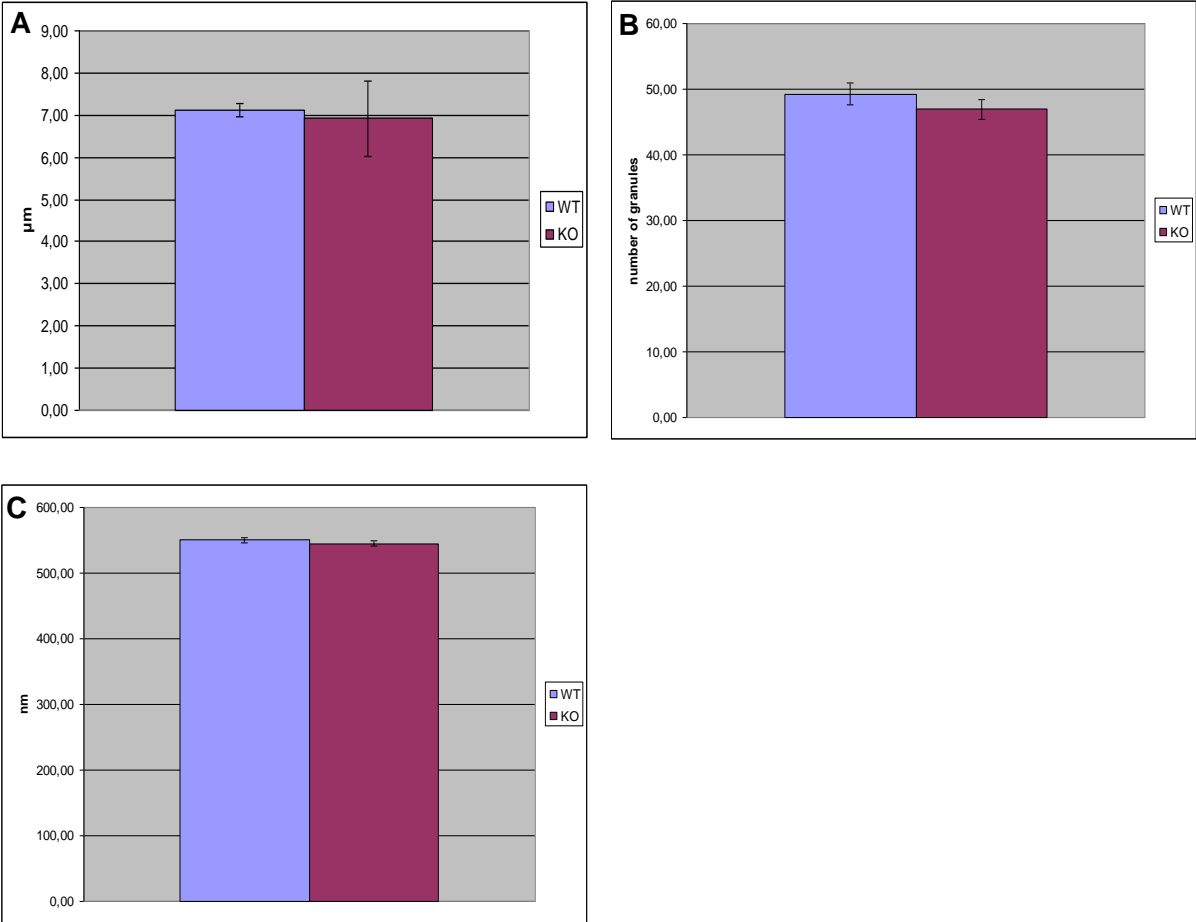


Figure 20: Mast cells parameters quantification results

The lack of difference between the CSP α KO and WT cells is been confirmed by quantifying A) the size of the cells; B) the number and C) diameter of the granules. Bars: average \pm s.e.m. For A) and B), n= 50 cells from 2 WT animals and 61 cells from 1 CSP α KO animal, for C) n=2463 granules from 2 WT mice and 2545 granules from 1 KO mouse.

4.6. CSP isoforms genotyping

CSP has three isoforms encoded by different genes: α , β and γ . CSP α is ubiquitously expressed, but highly enriched in brain, while CSP β and γ are testis specific. It has been shown that in some cells, like the inner hair cells, CSP β can act as a substitute for the lacking CSP α (Schmitz et al. 2006). To check for the presence of the other isoforms in the organs already examined with electron microscopy, total RNA was extracted from them and RT-PCR experiments were performed (see Materials and Methods, 3.5 and 3.6). As shown in Figure 21 and Figure 22, in all of the organs examined, CSP α is the only isoform present.

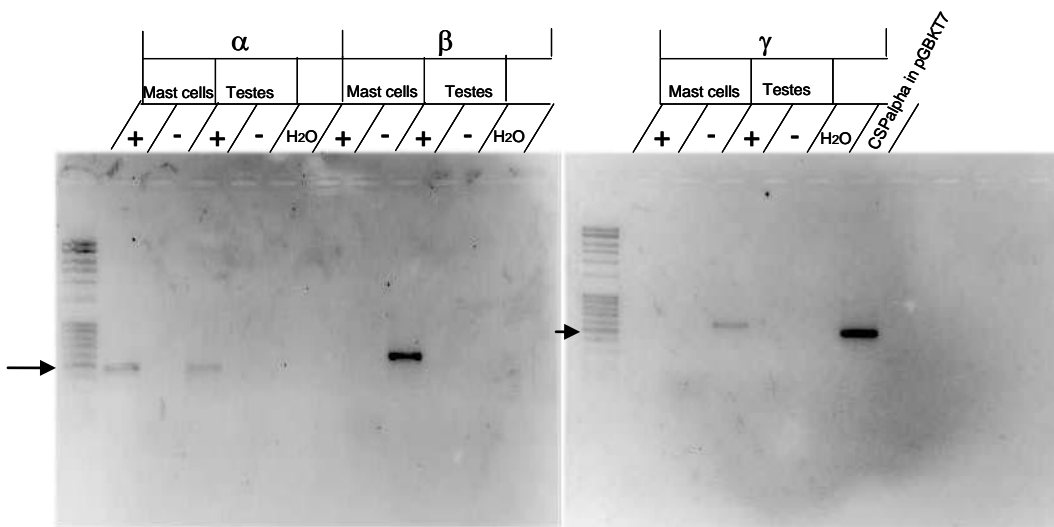


Figure 21: CSP Isotyping in the bone marrow mast cells

CSP α is the only isoform of CSP in the BMMC. Testis, which contains all of the isoforms, was used as positive control alongside with CSP α in pGBKT7 plasmid vector. +: reaction with reverse transcription, cDNA used as a template, -: reaction without reverse transcription, total RNA used as a template. Arrows point to 500bp band of the DNA standard. Expected size of bands: CSP α ~500bp, CSP β and γ ~600bp.

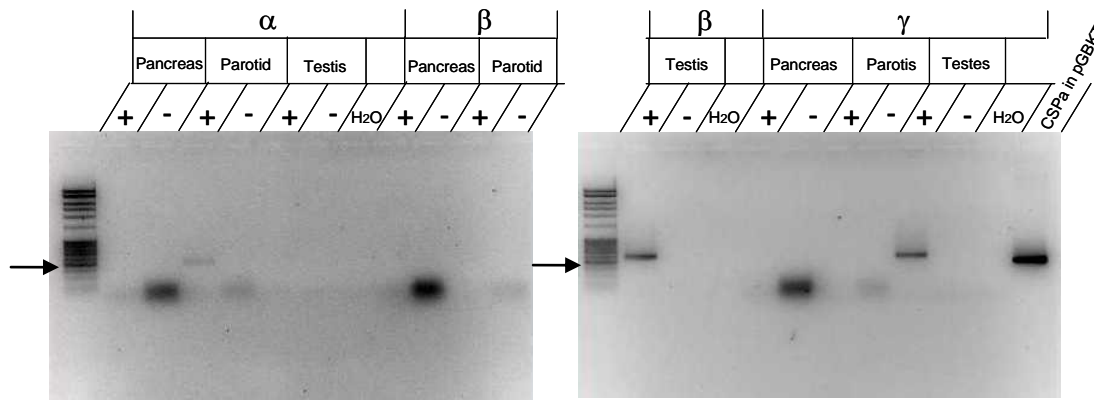


Figure 22: CSP Isotyping in the exocrine pancreas and the parotid gland

CSP α is the only isoform of CSP in the parotid gland. No band was detected in the pancreas. Testis used as positive control alongside with CSP α in pGBKT7 plasmid vector. +: reaction with reverse transcription, cDNA used as a template, -: reaction without reverse transcription, total RNA used as a template. Arrows point to 500bp band of the DNA standard. Expected size of bands: CSP α ~500bp, CSP β and γ ~600bp. Note: the thick bands at ~50bp are the primers used for the PCR.

Exocrine pancreas contains very high concentrations of RNase enzymes, which make RNA extraction and purification from it very difficult and in some cases impossible.

5. Discussion

CSP α KO mice are characterized by their progressive sensorimotor impairment as a result of the neurodegenerative processes taking place at the NMJ, Calyx of Held (Fernandez-Chacon et al. 2004) and photoreceptor synapses (Schmitz et al. 2006). Another characteristic of these KO mice is their inability to gain weight after the age of P15, and the very high rate of mortality, with none of the mutant mice surviving more than 3 months (Fernandez-Chacon et al. 2004). Inability to gain weight could be result of animals' disability to utilise the food as a result of alterations in the digestive tract. The exocrine glands of the digestive system (exocrine pancreas, parotid and submandibular gland) are essential for digestion. In the present study, I asked whether alterations are present in these exocrine glands in CSP α KO mice that could account for the dramatic inability to gain weight in these KO mice.

This study shows that, in deed, ultrastructural changes are present in the secretory glands, particularly the exocrine pancreas. In pancreatic acinar cells of CSP α KO mice there are more granules, which are bigger in diameter and are distributed widely across the cytoplasm. Some of the granules reach near the baso-lateral pole of the cell.

What could be the mechanism for the observed morphological changes is not clear. It is possible that due to the lack of the CSP α , these granules cannot be exocytosed and they accumulate into the cell. There, the granules could fuse among themselves (or with the lysosomes) and grow in size. CSP is implied to chaperone the SNARE complex (Chandra et al. 2005). The lack of CSP could decrease the formation of the SNARE complex, therefore exhibiting its effects on regulating the exocytosis. Without proper assembly of the SNAREs, the vesicles cannot be exocytosed and they

accumulate. As a support to this is the finding that the levels of SNAP-25, one of the members of the SNARE complex, are decreased by 30-40% in the CSP α KO mice. In addition, work on VAMP8/endobrevin KO mice (Wang et al. 2004) has indicated a major physiological role of VAMP8 in regulated exocytosis in exocrine pancreas, placing it as a member of the SNARE complex responsible for exocytosis in exocrine pancreas. VAMP8/endobrevin KO mice, similar to the CSP α KO mice, accumulate zymogen granules in the pancreatic acinar cells (Wang et al. 2004).

With the deletion of the CSP α , the SNAREs in the pancreas are not chaperoned, exocytosis is hindered and therefore the CSP α KO mice accumulate zymogen granules in the cytoplasm of the pancreatic acinar cells (Figure 5 and Figure 6). Nevertheless, the connection between CSP α chaperoning the SNAREs on one hand and the morphological changes in the pancreatic acinar cell on the other is still hypothetical, and needs further investigation.

In addition, CSP is known to take part in the recycling of Rab3 proteins (Sakisaka et al. 2002; Evans et al. 2003). In non-neuronal tissues, Rab3D is predominant isoform (Riedel et al. 2002). The analysis of Rab3D KO mice has suggested that Rab3D is not important for exocytosis, but for maintenance of normally sized granules in the pancreas and the parotid gland (Riedel et al. 2002). Similar to the CSP α KO mice, the pancreatic and parotid cells from the Rab3D KO mice have zymogen granules with bigger diameter when compared to their controls. In that study, it is suggested that Rab3D has an inhibitory effect on the granule-granule fusion and has a role in the maturation of the zymogen granules. In the absence of CSP α , the multi-protein chaperone complex that recycles Rab3D may not function properly. Therefore, Rab3D could not recycle and could not accomplish its effects upon the size-control of the granules. On the other hand, granule-granule fusion is mediated via different

members of the SNARE family (Wang et al. 2004), reviewed in (Gaisano 2000). These proteins may not be subject of CSP chaperone activity, thus avoiding the effects of CSP α deletion upon membrane fusion. Not being under control of CSP α activity, the granules can fuse among themselves, but not with the apical plasma membrane. This granule-granule fusion leads to increased diameter of the zymogen granules in the CSP α KO mice (Figure 5, Figure 7 and Figure 8). However, this remark is not supported by previous studies and is only hypothetical. It can serve as a starting point for future assessments.

The parotid and submandibular glands are exocrine glands of epithelial origin that contain secretory granules. The ultrastructural changes observed in the exocrine pancreas of CSP α KO mice, were in general, also observed in the parotid and submandibular glands (Figure 10, 11, 12, 13 and Figure 14, 16, 17 and 18). However, in the parotid gland, the acinar cells from the CSP α KO animals have *less* zymogen granules than the cells from the WT controls. This difference found in the parotid gland can be attributed to different development of the glands.

In particular, the development of the parotid gland is mouse strain-specific. Namely, in C57BL/6 mice (the background strain of the CSP α KO mice, (Fernandez-Chacon et al. 2004) the parotid gland reaches its full potential after the 3rd postnatal week (Domon and Kurabayashi 1987). At P17, the gland is not fully developed and is not fully functional. Therefore, the CSP α chaperone activity may not yet be necessary. Another point regarding the differences observed is that, although many of the SNARE isoforms have been identified in the parotid gland (Imai et al. 2001; Imai et al. 2003; Wang et al. 2007), it remains still uncertain whether the SNARE machinery is involved in the regulated exocytosis in the salivary glands (Takuma et al. 2000), for review, see (Turner and Sugiya 2002). Another possible explanation for the

heterogeneity of the observed morphological changes found is the expression of another CSP isoform in the parotid cell. As found in the inner hair cells of the CSP α KO mice, CSP β is expressed there and substitutes the deletion of CSP α (Schmitz et al. 2006). However, when searching for possible CSP isoforms in the parotid and submandibular glands used in this study, the CSP α was the only isoform found in all of them. It remains unclear why there is decrease in the number of granules in the parotid cells originating from the CSP α mutant mice.

For the submandibular gland, the proteins involved in regulating the exocytosis are not yet clear. In one study, it was even suggested that the secretion of amylase from this gland is probably a constitutive, non-regulated phenomenon, independent of extracellular or intracellular signals (Busch et al. 2002). So far, there are no reports of such gigantic granules (Figure 14 and Figure 15) found in the acinar cells of this gland in any mouse or other animal model. As mentioned above for the pancreas, the proteins responsible for inter-granular fusion might not be substrates for CSP α chaperone activity, therefore enabling zymogen granule-granule fusion (Figure 15), but not exocytosis and therefore enabling the accumulation of the zymogen granules in the cells.

Nevertheless, the exact molecular mechanisms of the membrane fusion in the submandibular gland remain to be addressed and the proteins involved in these processes to be discovered. This will shed light on the phenotype observed in the submandibular gland of the CSP α KO mice.

This study did not find any morphological changes in the peritoneal mast cells. This can be attributed to low number of experimental animals (1 KO and 2 WT mice) and to young age of the animals. According to unpublished data from a collaborative

laboratory, mast cells from CSP α KO mice show differences in exocytosis but evident in older age (after ~P30). Nevertheless, further experiments are necessary to inspect the role of CSP α in the mast cells functions.

The overall finding in the exocrine glands that not all of the cells are affected by the loss of CSP α is supportive to the theory that CSP α acts in a chaperone manner. Physiologically, some cells exhibit higher levels of activity than others do. In those parts (or cells) of the organ with higher activity, it is logical that the relevant proteins are exposed to higher stress. Consequently, they age sooner and become unable to perform their roles. Lacking the chaperone machinery, their recycling is hindered. Because of this, the effects of the CSP α deletion become obvious sooner or to greater extent in these cells than in those that have lower levels of activity. This could explain why some cells in the CSP α KO animals' glands have normal values of their parameters (Figure 6, 7 and 9 for pancreas, Figure 11, 12 and 13 for parotid and Figure 16, 17 and 18 for submandibular gland).

6. Conclusion

This study aimed at identifying possible defects in the digestive tract of the CSP α KO mice, which can be responsible for the animals' inability to gain weight. Morphological changes are present in the exocrine glands of the digestive system, which are indicative for pathological processes. These findings occur as a result of "removing" the CSP α chaperone activity, rendering decreased SNARE complex formation (thus accumulation of granules) and decreased control of Rab3D recycling (thus increased size of the granules). However, the exact cellular mechanisms of these effects are not subject of this study and remain to be addressed in future experimental work. Furthermore, the CSP α KO mice could die as a consequence of the changes observed in the exocrine glands of the digestive system, but considering the ubiquitous expression of CSP α , it is possible that they die of yet unidentified dysfunction of some of the animals' organs.

7. References

- Arnold, C., N. Reisch, C. Leibold, S. Becker, K. Prufert, K. Sautter, D. Palm, S. Jatzke, S. Buchner and E. Buchner (2004). "Structure-function analysis of the cysteine string protein in *Drosophila*: cysteine string, linker and C terminus." J Exp Biol **207**(Pt 8): 1323-34.
- Blank, U., B. Cyprien, S. Martin-Verdeaux, F. Paumet, I. Pombo, J. Rivera, M. Roa and N. Varin-Blank (2002). "SNAREs and associated regulators in the control of exocytosis in the RBL-2H3 mast cell line." Mol Immunol **38**(16-18): 1341-5.
- Boal, F., H. Zhang, C. Tessier, P. Scotti and J. Lang (2004). "The variable C-terminus of cysteine string proteins modulates exocytosis and protein-protein interactions." Biochemistry **43**(51): 16212-23.
- Braun, J. E., B. A. Fritz, S. M. Wong and A. W. Lowe (1994). "Identification of a vesicle-associated membrane protein (VAMP)-like membrane protein in zymogen granules of the rat exocrine pancreas." J Biol Chem **269**(7): 5328-35.
- Braun, J. E. and R. H. Scheller (1995). "Cysteine string protein, a DnaJ family member, is present on diverse secretory vesicles." Neuropharmacology **34**(11): 1361-9.
- Braun, J. E., S. M. Wilbanks and R. H. Scheller (1996). "The cysteine string secretory vesicle protein activates Hsc70 ATPase." J Biol Chem **271**(42): 25989-93.
- Brown, H., O. Larsson, R. Branstrom, S. N. Yang, B. Leibiger, I. Leibiger, G. Fried, T. Moede, J. T. Deeney, G. R. Brown, G. Jacobsson, C. J. Rhodes, J. E. Braun, R. H. Scheller, B. E. Corkey, P. O. Berggren and B. Meister (1998). "Cysteine string protein (CSP) is an insulin secretory granule-associated protein regulating beta-cell exocytosis." Embo J **17**(17): 5048-58.
- Busch, L., L. Sterin-Borda and E. Borda (2002). "Differences in the regulatory mechanism of amylase release by rat parotid and submandibular glands." Archives of Oral Biology **47**(10): 717-722.

- Caplan, A. J., D. M. Cyr and M. G. Douglas (1993). "Eukaryotic homologues of Escherichia coli DnaJ: a diverse protein family that functions with hsp70 stress proteins." Mol Biol Cell **4**(6): 555-63.
- Chamberlain, L. H. and R. D. Burgoyne (1997). "Activation of the ATPase activity of heat-shock proteins Hsc70/Hsp70 by cysteine-string protein." Biochem J **322** (Pt 3): 853-8.
- Chamberlain, L. H. and R. D. Burgoyne (1997). "The molecular chaperone function of the secretory vesicle cysteine string proteins." J Biol Chem **272**(50): 31420-6.
- Chamberlain, L. H. and R. D. Burgoyne (1998). "The cysteine-string domain of the secretory vesicle cysteine-string protein is required for membrane targeting." Biochem J **335** (Pt 2): 205-9.
- Chamberlain, L. H. and R. D. Burgoyne (2000). "Cysteine-string protein: the chaperone at the synapse." J Neurochem **74**(5): 1781-9.
- Chandra, S., G. Gallardo, R. Fernandez-Chacon, O. M. Schluter and T. C. Südhof (2005). "Alpha-synuclein cooperates with CSPalpha in preventing neurodegeneration." Cell **123**(3): 383-96.
- Cheetham, M. E. and A. J. Caplan (1998). "Structure, function and evolution of DnaJ: conservation and adaptation of chaperone function." Cell Stress Chaperones **3**(1): 28-36.
- Chen, S., X. Zheng, K. L. Schulze, T. Morris, H. Bellen and E. F. Stanley (2002). "Enhancement of presynaptic calcium current by cysteine string protein." J Physiol **538**(Pt 2): 383-9.
- Cook, L. J., O. A. Musa and R. M. Case (1996). "Intracellular transport of pancreatic enzymes." Scand J Gastroenterol Suppl **219**: 1-5.
- Cosen-Binker, L. I. and H. Y. Gaisano (2007). "Recent insights into the cellular mechanisms of acute pancreatitis." Can J Gastroenterol **21**(1): 19-24.

- Dawson-Scully, K., P. Bronk, H. L. Atwood and K. E. Zinsmaier (2000). "Cysteine-string protein increases the calcium sensitivity of neurotransmitter exocytosis in *Drosophila*." J Neurosci **20**(16): 6039-47.
- Domon, M. and T. Kurabayashi (1987). "Postnatal development of the duct system in the mouse parotid gland." Anat Rec **217**(4): 391-4.
- Evans, G. J. and A. Morgan (2002). "Phosphorylation-dependent interaction of the synaptic vesicle proteins cysteine string protein and synaptotagmin I." Biochem J **364**(Pt 2): 343-7.
- Evans, G. J., A. Morgan and R. D. Burgoyne (2003). "Tying everything together: the multiple roles of cysteine string protein (CSP) in regulated exocytosis." Traffic **4**(10): 653-9.
- Fernandez-Chacon, R., M. Wolfel, H. Nishimune, L. Tabares, F. Schmitz, M. Castellano-Munoz, C. Rosenmund, M. L. Montesinos, J. R. Sanes, R. Schneggenburger and T. C. Südhof (2004). "The synaptic vesicle protein CSP alpha prevents presynaptic degeneration." Neuron **42**(2): 237-51.
- Gaisano, H. Y. (2000). "A hypothesis: SNARE-ing the mechanisms of regulated exocytosis and pathologic membrane fusions in the pancreatic acinar cell." Pancreas **20**(3): 217-26.
- Gaisano, H. Y., L. Sheu, G. Grondin, M. Ghai, A. Bouquillon, A. Lowe, A. Beaudoin and W. S. Trimble (1996). "The vesicle-associated membrane protein family of proteins in rat pancreatic and parotid acinar cells." Gastroenterology **111**(6): 1661-9.
- Gaisano, H. Y., L. Sheu, P. P. Wong, A. Klip and W. S. Trimble (1997). "SNAP-23 is located in the basolateral plasma membrane of rat pancreatic acinar cells." FEBS Lett **414**(2): 298-302.
- Graham, M. E. and R. D. Burgoyne (2000). "Comparison of cysteine string protein (Csp) and mutant alpha-SNAP overexpression reveals a role for csp in late steps of membrane fusion in dense-core granule exocytosis in adrenal chromaffin cells." J Neurosci **20**(4): 1281-9.

- Gundersen, C. B., A. Mastrogiacomo, K. Faull and J. A. Umbach (1994). "Extensive lipidation of a Torpedo cysteine string protein." J Biol Chem **269**(30): 19197-9.
- Gundersen, C. B. and J. A. Umbach (1992). "Suppression cloning of the cDNA for a candidate subunit of a presynaptic calcium channel." Neuron **9**(3): 527-37.
- Hansen, N. J., W. Antonin and J. M. Edwardson (1999). "Identification of SNAREs involved in regulated exocytosis in the pancreatic acinar cell." J Biol Chem **274**(32): 22871-6.
- Hartl, F. U. and M. Hayer-Hartl (2002). "Molecular chaperones in the cytosol: from nascent chain to folded protein." Science **295**(5561): 1852-8.
- Hsu, C. C., K. M. Davis, H. Jin, T. Foos, E. Floor, W. Chen, J. B. Tyburski, C. Y. Yang, J. V. Schloss and J. Y. Wu (2000). "Association of L-glutamic acid decarboxylase to the 70-kDa heat shock protein as a potential anchoring mechanism to synaptic vesicles." J Biol Chem **275**(27): 20822-8.
- Imai, A., T. Nashida and H. Shimomura (2001). "mRNA expression of membrane-fusion-related proteins in rat parotid gland." Arch Oral Biol **46**(10): 955-62.
- Imai, A., T. Nashida, S. Yoshie and H. Shimomura (2003). "Intracellular localisation of SNARE proteins in rat parotid acinar cells: SNARE complexes on the apical plasma membrane." Arch Oral Biol **48**(8): 597-604.
- Jacobsson, G. and B. Meister (1996). "Molecular components of the exocytotic machinery in the rat pituitary gland." Endocrinology **137**(12): 5344-56.
- Kelley, W. L. (1998). "The J-domain family and the recruitment of chaperone power." Trends Biochem Sci **23**(6): 222-7.
- Leveque, C., S. Pupier, B. Marqueze, L. Geslin, M. Kataoka, M. Takahashi, M. De Waard and M. Seagar (1998). "Interaction of cysteine string proteins with the alpha1A subunit of the P/Q-type calcium channel." J Biol Chem **273**(22): 13488-92.

- Logan, M. R., S. O. Odemuyiwa and R. Moqbel (2003). "Understanding exocytosis in immune and inflammatory cells: the molecular basis of mediator secretion." J Allergy Clin Immunol **111**(5): 923-32; quiz 933.
- Luan, P., W. E. Balch, S. D. Emr and C. G. Burd (1999). "Molecular dissection of guanine nucleotide dissociation inhibitor function in vivo. Rab-independent binding to membranes and role of Rab recycling factors." J Biol Chem **274**(21): 14806-17.
- Magga, J. M., S. E. Jarvis, M. I. Arnot, G. W. Zamponi and J. E. Braun (2000). "Cysteine string protein regulates G protein modulation of N-type calcium channels." Neuron **28**(1): 195-204.
- Mastrogiacomo, A. and C. B. Gundersen (1995). "The nucleotide and deduced amino acid sequence of a rat cysteine string protein." Brain Res Mol Brain Res **28**(1): 12-8.
- Mastrogiacomo, A., S. M. Parsons, G. A. Zampighi, D. J. Jenden, J. A. Umbach and C. B. Gundersen (1994). "Cysteine string proteins: a potential link between synaptic vesicles and presynaptic Ca²⁺ channels." Science **263**(5149): 981-2.
- Matos, M. F., J. Rizo and T. C. Südhof (2000). "The relation of protein binding to function: what is the significance of munc18 and synaptotagmin binding to syntaxin 1, and where are the corresponding binding sites?" Eur J Cell Biol **79**(6): 377-82.
- Morales, M., A. Ferrus and M. Martínez-Padron (1999). "Presynaptic calcium-channel currents in normal and csp mutant *Drosophila* peptidergic terminals." Eur J Neurosci **11**(5): 1818-26.
- Nie, Z., R. Ranjan, J. J. Wenniger, S. N. Hong, P. Bronk and K. E. Zinsmaier (1999). "Overexpression of cysteine-string proteins in *Drosophila* reveals interactions with syntaxin." J Neurosci **19**(23): 10270-9.
- Ohyama, T., P. Verstreken, C. V. Ly, T. Rosenmund, A. Rajan, A. C. Tien, C. Haueter, K. L. Schulze and H. J. Bellen (2007). "Huntingtin-interacting protein 14, a palmitoyl transferase required for exocytosis and targeting of CSP to synaptic vesicles." J Cell Biol **179**(7): 1481-96.

- Palade, G. (1975). "Intracellular Aspects of the Process of Protein Synthesis." Science **189**(4206): 867.
- Pickett, J. A. and J. M. Edwardson (2006). "Compound exocytosis: mechanisms and functional significance." Traffic **7**(2): 109-16.
- Ranjan, R., P. Bronk and K. E. Zinsmaier (1998). "Cysteine string protein is required for calcium secretion coupling of evoked neurotransmission in drosophila but not for vesicle recycling." J Neurosci **18**(3): 956-64.
- Ribeiro, R. A., M. L. Vale, S. M. Thomazzi, A. B. Paschoalato, S. Poole, S. H. Ferreira and F. Q. Cunha (2000). "Involvement of resident macrophages and mast cells in the writhing nociceptive response induced by zymosan and acetic acid in mice." Eur J Pharmacol **387**(1): 111-8.
- Riedel, D., W. Antonin, R. Fernández-Chacón, G. Alvarez de Toledo, T. Jo, M. Geppert, J. A. Valentijn, K. Valentijn, J. D. Jamieson, T. C. Südhof and R. Jahn (2002). "Rab3D is not required for exocrine exocytosis but for maintenance of normally sized secretory granules." Mol Cell Biol **22**(18): 6487-97.
- Sakisaka, T., T. Meerlo, J. Matteson, H. Plutner and W. E. Balch (2002). "Rab-alphaGDI activity is regulated by a Hsp90 chaperone complex." Embo J **21**(22): 6125-35.
- Schmitz, F., L. Tabares, D. Khimich, N. Strenzke, P. de la Villa-Polo, M. Castellano-Muñoz, A. Bulankina, T. Moser, R. Fernández-Chacón and T. C. Südhof (2006). "CSPalpha-deficiency causes massive and rapid photoreceptor degeneration." Proc Natl Acad Sci U S A **103**(8): 2926-31.
- Silver, P. A. and J. C. Way (1993). "Eukaryotic DnaJ homologs and the specificity of Hsp70 activity." Cell **74**(1): 5-6.
- Stahl, B., S. Tobaben and T. C. Südhof (1999). "Two distinct domains in hsc70 are essential for the interaction with the synaptic vesicle cysteine string protein." Eur J Cell Biol **78**(6): 375-81.

- Stevens, A. and J. Lowe (1992). Histology. London, New York, Gower Medical Publishing
- Takuma, T., T. Arakawa and Y. Tajima (2000). "Interaction of SNARE proteins in rat parotid acinar cells." Arch Oral Biol **45**(5): 369-75.
- Tobaben, S., P. Thakur, R. Fernandez-Chacon, T. C. Südhof, J. Rettig and B. Stahl (2001). "A trimeric protein complex functions as a synaptic chaperone machine." Neuron **31**(6): 987-99.
- Turner, R. J. and H. Sugiya (2002). "Understanding salivary fluid and protein secretion." Oral Dis **8**(1): 3-11.
- Umbach, J. A., K. E. Zinsmaier, K. K. Eberle, E. Buchner, S. Benzer and C. B. Gundersen (1994). "Presynaptic dysfunction in *Drosophila* csp mutants." Neuron **13**(4): 899-907.
- van de Goor, J. and R. B. Kelly (1996). "Association of *Drosophila* cysteine string proteins with membranes." FEBS Lett **380**(3): 251-6.
- Vennekens, R., J. Olausson, M. Meissner, W. Bloch, I. Mathar, S. E. Philipp, F. Schmitz, P. Weissgerber, B. Nilius, V. Flockerzi and M. Freichel (2007). "Increased IgE-dependent mast cell activation and anaphylactic responses in mice lacking the calcium-activated nonselective cation channel TRPM4." Nat Immunol **8**(3): 312-20.
- Wang, C. C., C. P. Ng, L. Lu, V. Atlashkin, W. Zhang, L. F. Seet and W. Hong (2004). "A role of VAMP8/endobrevin in regulated exocytosis of pancreatic acinar cells." Dev Cell **7**(3): 359-71.
- Wang, C. C., H. Shi, K. Guo, C. P. Ng, J. Li, B. Q. Gan, H. Chien Liew, J. Leinonen, H. Rajaniemi, Z. H. Zhou, Q. Zeng and W. Hong (2007). "VAMP8/endobrevin as a general vesicular SNARE for regulated exocytosis of the exocrine system." Mol Biol Cell **18**(3): 1056-63.
- Williams, J. A. (2001). "Intracellular signaling mechanisms activated by cholecystokinin-regulating synthesis and secretion of digestive enzymes in pancreatic acinar cells." Annu Rev Physiol **63**: 77-97.

- Williams, J. A. (2006). "Regulation of pancreatic acinar cell function." Curr Opin Gastroenterol **22**(5): 498-504.
- Winnefeld, M., J. Rommelaere and C. Cziepluch (2004). "The human small glutamine-rich TPR-containing protein is required for progress through cell division." Exp Cell Res **293**(1): 43-57.
- Zerial, M. and H. McBride (2001). "Rab proteins as membrane organizers." Nat Rev Mol Cell Biol **2**(2): 107-17.
- Zhang, H., W. L. Kelley, L. H. Chamberlain, R. D. Burgoyne and J. Lang (1999). "Mutational analysis of cysteine-string protein function in insulin exocytosis." J Cell Sci **112 (Pt 9)**: 1345-51.
- Zhang, H., W. L. Kelley, L. H. Chamberlain, R. D. Burgoyne, C. B. Wollheim and J. Lang (1998). "Cysteine-string proteins regulate exocytosis of insulin independent from transmembrane ion fluxes." FEBS Lett **437**(3): 267-72.
- Zinsmaier, K. E., K. K. Eberle, E. Buchner, N. Walter and S. Benzer (1994). "Paralysis and early death in cysteine string protein mutants of *Drosophila*." Science **263**(5149): 977-80.
- Zinsmaier, K. E., A. Hofbauer, G. Heimbeck, G. O. Pflugfelder, S. Buchner and E. Buchner (1990). "A cysteine-string protein is expressed in retina and brain of *Drosophila*." J Neurogenet **7**(1): 15-29.

8. Acknowledgements

I would like to express my gratitude to Prof. Dr. Frank Schmitz for giving me the opportunity to enter the scientific community and for his guidance, confidence and patience.

I would like to thank Dr. Ivan Bogeski for his limitless support during my thesis work.

I am very grateful to Gabi Kiefer and Gerlinde Kühnreich for introducing me to the details of the Electron Microscopy techniques. In addition, I would like to express my gratitude to Venkat Giri Magupalli, Kannan Alpadi, Dr. Karin Schwarz, Jagadeesh Venkatesian, Sivaraman Natarajan and Sylvia Brundaler for their friendship, advices and help.

I wish to express my deepest gratitude to my family, especially to my wife Julija and my late father Ilija, for the never-ending support.

Thank you all!

9. Curriculum Vitae

Name

Josif Mirceski

Date and place of birth

16.10.1979 in Prilep, Republic of Macedonia

Education

Doctorate in Medicine (Dr. med) (2005 to present)

Institute for Anatomy and Cell Biology, Dept. of Neuroanatomy, University of Saarland, Germany

Masters in Medicine

Medical Faculty, Medical University Pleven, Bulgaria (1998- 2005)

Primary and secondary school

Prilep, Republic of Macedonia (1986-1998)

Research experience

MD thesis (2005 till present)

“Characterization of CSPalpha KO mice”- ultrastructural morphological investigation of exocrine secretory glands of the digestive system

Prof. Dr. Frank Schmitz Dept. of Neuroanatomy Institute for Anatomy and Cell Biology, University of Saarland (UdS), Homburg, Germany

German-Spanish collaborative research exchange program

Prof. Dr. Rafael Fernandez-Chacon, Department of Physiology, University of Seville, Spain

Teaching experience

Tutor- Gross Anatomy course for the medical students at the University of Saarland

Tutor- Electron Microscopy techniques for the Graduate Program “Ca²⁺ signalling and cellular nanodomains” at the University of Saarland

Professional experience

Physician training-Departments of Internal Medicine and Urology, General Hospital in Prilep, Macedonia (2005)

Technical experience

Electron microscopy techniques- TEM and tomography

Light microscopy, Fluorescence and Confocal microscopy

Live cell imaging- Time lapse microscopy

Handling and surgery of laboratory animals

Electrophysiology (whole-cell patch clamping)

Basic molecular biology techniques